Title

Cross-species functional diversity within the PIN auxin efflux protein family

Authors

Devin Lee O'Connor[1,^], Mon Mandy Hsia[2], John Vogel[3,4], Ottoline Leyser[1].

Affiliations

[1]Sainsbury Laboratory University of Cambridge, Cambridge, UK.

[2]USDA-ARS Western Regional Research Center, Albany, CA.

[3]U.S. Department of Energy Joint Genome Institute, Walnut Creek, CA.

[4]Department of Plant and Microbial Biology, University of California, Berkeley, CA.

^Author for Correspondence: Devin Lee O'Connor devin.oconnor@slcu.cam.ac.uk

Abstract

In plants, directional transport of the hormone auxin creates concentration maxima and paths of transport that provide positional, polarity, and growth regulatory cues throughout development. In *Arabidopsis thaliana,* the polar-localized auxin efflux protein PIN-FORMED1 (AtPIN1) is required to coordinate development during flowering. However, Arabidopsis has a derived PIN family structure; the majority of flowering plants have retained a clade of PIN proteins phylogenetically sister to PIN1, the Sister-of-PIN1 clade (SoPIN1), which has been lost in the Brassicaceae, including Arabidopsis. Based on PIN localization in the grasses *Brachypodium distachyon* and *Zea mays*, which have both SoPIN1 and PIN1 clades, we previously proposed that the organ initiation and vein patterning roles attributed to AtPIN1 were shared between the SoPIN1 and PIN1 clades in grasses. Here we show that *sopin1* and *pin1b* mutants have distinct phenotypes in Brachypodium. *sopin1* mutants have severe organ initiation defects similar to Arabidopsis *atpin1* mutants, while *pin1b* mutants initiate organs normally but have increased stem elongation. Heterologous expression of Brachypodium PIN1b and SoPIN1 in Arabidopsis *atpin1* mutants provides further evidence for functional distinction between the two clades. SoPIN1 but not PIN1b can complement null *atpin1* mutants, while both PINs can complement an *atpin1* missense allele with a single amino acid change. The different localization behaviors of SoPIN1 and PIN1b when heterologously expressed in Arabidopsis provide insight into how PIN accumulation at the plasma membrane, tissue-level protein accumulation, transport activity, and interaction, all contribute to the polarization dynamics that distinguish PIN family members. Combined, these results suggest that the PIN polarization and trafficking behaviors required for organ initiation differ from those

required for other PIN functions in the shoot, and that in most flowering plants these functions are split between two PIN clades.

Introduction

The plant hormone auxin is an essential mobile signal controlling growth and patterning throughout plant development (Leyser, 2010). Auxin can passively enter cells, triggering a vast array of downstream signaling events (Wang and Estelle, 2014), but it cannot easily exit the cell without active transport (Raven, 1975; Rubery and Sheldrake, 1974). As a result, directional efflux mediated by the polar-localized PIN-FORMED (PIN) efflux carriers can organize auxin accumulation patterns, creating concentration maxima and paths of transport that regulate growth, position organs, and pattern tissues (Adamowski and Friml, 2015). Because auxin itself feeds back to regulate PIN-mediated transport both transcriptionally and post-transcriptionally (Leyser, 2006), the transport system shows remarkable robustness and plasticity. For example, compensatory changes in PIN abundance between PIN family members can mitigate PIN loss-of-function mutant phenotypes (Blilou et al., 2005; Paponov et al., 2005; Vieten et al., 2005), environmental inputs can trigger tissue-level changes in PIN abundance and polarity leading to altered plant growth (Habets and Offringa, 2014), and auxin transport paths can be reorganized in response to injury (Xu et al., 2006), or spontaneously in tissue culture (Gordon et al., 2007). The self-organizing properties of the auxin transport system thus gives this patterning mechanism extraordinary versatility, and allows it to coordinate local and long range communication in the plant.

The correct initiation and positioning of organs (leaves, flowers, stems) in the growing tip, or shoot apical meristem, of *Arabidopsis thaliana* (Arabidopsis) plants requires the

action of the PIN-FORMED1 (AtPIN1) auxin efflux carrier (Okada et al., 1991). AtPIN1 is targeted to the plasma membrane and polarized in cells (Gälweiler et al., 1998). In the meristem epidermis, polarization of AtPIN1 in neighboring cells converges around the initiation sites of new organs, suggesting that polarized AtPIN1 concentrates auxin into local maxima causing organ initiation (Benková et al., 2003; Heisler et al., 2005; Reinhardt et al., 2003). Accordingly, in *atpin1* loss-of-function mutants, or if auxin transport is pharmacologically inhibited, organ initiation is aborted, but it can be rescued with local auxin application to the meristem flank (Reinhardt et al., 2003; Reinhardt et al., 2000). Organ initiation in *atpin1* mutants can also be rescued with epidermal-specific AtPIN1 expression (Bilsborough et al., 2011) and reducing AtPIN1 function specifically in the epidermis compromises organ positioning and initiation (Kierzkowski et al., 2013), demonstrating the importance of convergent AtPIN1 polarization in the epidermis during organ formation.

The recurrent formation of AtPIN1 convergence points surrounding auxin maxima in the meristem epidermis has been the focus of several computational models that attempt to explain how auxin feeds back on its own transport via AtPIN1 to concentrate auxin and control organ spacing (Abley et al., 2016; Bayer et al., 2009; Bhatia et al., 2016; Heisler et al., 2010; Jönsson et al., 2006; Smith et al., 2006; Stoma et al., 2008). However, AtPIN1 is also expressed during the patterning of the vascular strands formed coincident with organ positioning, and in these sub-epidermal cells AtPIN1 is polarized basally, away from the presumed auxin maxima, suggesting that the control of AtPIN1 polarity with respect to auxin is not consistent across tissues (Bayer et al., 2009).

Indeed, AtPIN1 has several functions post-initiation that are not necessarily associated with convergent polarization patterns (Gälweiler et al., 1998; Scarpella et

al., 2006). During the vegetative phase, AtPIN1 is not required for organ initiation, but the organs that do form are misplaced and have severe morphological and vascular defects similar to those observed upon pharmacological inhibition of auxin transport, suggesting an important role for AtPIN1 in post-initiation morphogenesis and vein patterning in leaves (Guenot et al., 2012; Sawchuk et al., 2013; Verna et al., 2015). Furthermore, in mature tissues, AtPIN1 is polarized basally (root-ward) in vascular-associated cells and is required for efficient long distance transport of auxin down the shoot in the polar auxin transport stream, and this has been proposed to play an important role in the regulation of shoot branching (Bennett et al., 2016; Bennett et al., 2006; Gälweiler et al., 1998; Shinohara et al., 2013). Mutations in other PIN family members in combination with *atpin1* mutants suggest further functions in embryo development, root development and during plant growth responses to light and gravity (Leyser, 2005). Unfortunately, the myriad roles for AtPIN1 during plant development are genetically obscured by the severity of *atpin1* organ initiation defects.

We previously showed that all sampled flowering plants outside of the Brassicacea family have a clade of PIN proteins sister to the PIN1 clade (The Sister-of-PIN1 or SoPIN1 clade), while Arabidopsis and other Brassicacea species have lost this clade (O'Connor et al., 2014). During organ initiation in the grass *Brachypodium distachyon* (Brachypodium) SoPIN1 is highly expressed in the epidermis, polarizes towards presumed auxin maxima, and forms convergent polarization patterns during the formation of new organs, suggesting a role in creating the auxin maxima required for organ initiation. In contrast, the PIN1 clade members in Brachypodium, PIN1a and PIN1b, are not highly expressed in the epidermis, orient away from presumed auxin maxima, and are primarily expressed during patterning in the sub-epidermal tissues. Thus, the combined expression domains and polarization behaviors of SoPIN1,

PIN1a, and PIN1b in Brachypodium largely recapitulate those observed for AtPIN1 in Arabidopsis.

The localization and polarization of the Brachypodium SoPIN1 and PIN1 clades can be modeled with two different polarization modes with respect to auxin; SoPIN1 polarizes “up-the-gradient”, towards the neighboring cell with the highest auxin concentration, while PIN1a and PIN1b polarize “with-the-flux”, accumulating in the membrane with the highest auxin flux (O'Connor et al., 2014). Both polarization modes were previously applied to AtPIN1 in order to capture the switch in polarity observed during organ initiation and vein patterning, first orienting toward auxin maxima during convergence point formation, then orienting away from maxima during vein patterning below the epidermis (Bayer et al., 2009). These localization and modeling results suggest that in most angiosperm species the organ placement and vascular patterning functions attributed to AtPIN1 in Arabidopsis are split between the PIN1 and SoPIN1 clades, and that these two clades have different polarization properties with respect to auxin.

Here we present the functional analysis of both SoPIN1 and PIN1 protein clade members in Brachypodium, a species with the canonical two-clade family structure. We show that SoPIN1 and PIN1b have different functions during Brachypodium development, with SoPIN1 being required for organ initiation during the flowering phase, and PIN1b regulating stem elongation. Using heterologous expression in Arabidopsis, we show that the two proteins have different accumulation, polarization and transport behaviors that result in different functional properties independent of transcriptional context. In addition to elucidating several ways in which PIN family members can be functionally distinct, these results suggest that the Arabidopsis AtPIN1 protein represents an example of an evolutionary phenomenon the opposite

of subfunctionalisation in which protein functions are amalgamated into a single protein rather than diversified amongst paralogs. AtPIN1 has a repertoire of roles, and associated polarization behaviors that are distributed among several clades of PIN proteins in most flowering plants.

Results

SoPIN1 and PIN1b have different functions in Brachypodium

During organ formation in the Brachypodium shoot, both SoPIN1 and PIN1b expression precede PIN1a, which only accumulates significantly at the site of vein formation after the organ begins to grow. In the earliest stages of initiation, prior to the periclinal cell divisions that are the hallmark of morphogenesis, SoPIN1 forms convergent polarization patterns around the presumed auxin maxima in the meristem epidermis, while PIN1b is expressed internally and orients away from the maxima (O'Connor et al., 2014). Because of their early expression and opposing polarization patterns, we focused on characterizing SoPIN1 and PIN1b as representatives of the SoPIN1 and PIN1 clades.

We targeted Brachypodium SoPIN1 and PIN1b with CRISPR and recovered loss-of-function mutants in both genes (see methods). Both *sopin1-1* and *pin1b-1* mutants have single base-pair lesions that result in frame-shifts and premature stop codons (Figure 1A). *sopin1-1* mutants show severe organ initiation defects in the inflorescence remarkably similar to loss-of-function *atpin1* mutants in *Arabidopsis* (Figure 1B-C, Figure 1 – supplement 1)(Okada et al., 1991). The indeterminate flowering shoots of the Brachypodium inflorescence, called spikelets (Figure 1B, inset), often fail to initiate in *sopin1-1* despite sometimes clear definition of node vs internode tissue (n, and i, in

158 Figure 1C). When spikelets do form, the spikelet meristems are often devoid of new
159 organs (Arrows in Figure 1C inset).

160 In wildtype spikelet meristems, SoPIN1 convergence point formation is coincident with
161 a decrease in the nuclear auxin response reporter protein DII-Venus (Brunoud et al.,
162 2012) (DII) (Figure 1E), which functions in Brachypodium and is degraded in the
163 presence of auxin in spikelet meristems (Figure 1 - supplement 2). In *sopin1-1*
164 meristems DII accumulation is uniformly high for long stretches of the epidermis, and
165 the patterned reduction of DII both in the meristem epidermis and internally fails to
166 occur, suggesting a failure to organize auxin maxima (Figure 1F arrow).

167 In contrast to the severe defects of *sopin1-1*, organ initiation in *pin1b-1* mutants is
168 unaffected (Figure 1D). However, *pin1b-1* mutants show minor shoot twisting and
169 increased internode (stem tissue) length, especially in the basal few internodes
170 (Figure 1G, 1H). The longer internodes of *pin1b-1* lead to an overall increase in plant
171 height (Figure 1H). The internode defects of *pin1-b* are consistent with the abundant
172 PIN1b accumulation observed in wildtype stem tissue (Figure 1I). The difference in
173 phenotypes between *sopin1-1* and *pin1b-1* Brachypodium mutants suggests a
174 functional distinction between the SoPIN1 and PIN1 clades, and indicates that while
175 PIN1b is expendable for organ initiation, it is involved in the regulation of internode
176 growth.

177

SoPIN1 and PIN1b accumulate differently in Arabidopsis

The difference between the *sopin1-1* and *pin1b-1* phenotypes in Brachypodium may be due to their different expression patterns and not necessarily to differences in polarization behavior as previously hypothesized (O'Connor et al., 2014). In order to determine the functional differences that exist between the proteins themselves, we expressed both Brachypodium proteins in wildtype (Columbia, Col-0) Arabidopsis under the control of a 3.5kb Arabidopsis *PIN1* promoter fragment known to drive PIN1 expression sufficient to complement *pin1* mutants (*proAtPIN1*) (Heisler et al., 2005). Remarkably, despite the loss of SoPIN1 from Arabidopsis, Brachypodium SoPIN1 created clear convergent polarization patterns around the sites of organ initiation in Arabidopsis inflorescence meristems (Figure 2I asterisk, 25 of 27 meristems from 4 independent transgenic events). SoPIN1 protein abundance was highest in the meristem epidermis and SoPIN1 convergence points were most clearly observed surrounding I2 and I1 primordia (Figure 2A). Immediately below the apex, SoPIN1 accumulated in an ill-defined ring shape within which the vascular bundles will form (Figure 2J, 15 of 23 meristems from 4 independent transgenic events).

In contrast, significant PIN1b accumulation was absent from the meristem epidermis in 19 of 29 meristems from 7 independent transgenic events. In the few meristems where PIN1b was significantly expressed in the epidermis, it did not show clear convergent polarization patterns, and its polarity was often unclear (Figure 2B). Within initiating organs PIN1b often localized to punctate vesicular bodies inside cells, not the cell membrane (Figure 2B arrow). The PIN1b expression level remained low just below the meristem apex, but in contrast to SoPIN1, PIN1b formed defined domains around the presumptive developing vascular bundles (Figure 2L). The lack of PIN1b

protein in the meristem epidermis was not due to silencing of the transgene in these lines because we observed abundant PIN1b protein in the developing vasculature below the apex, even in plants where the meristem had no epidermal expression (Figure 2D) (8 samples from 4 events). In the same tissues SoPIN1 accumulated in both the vasculature and the epidermis (Figure 2C) (5 samples from 2 events).

In order to determine whether there were similar tissue-level differences in protein accumulation in mature tissues, we imaged SoPIN1 and PIN1b in the basal internode. Here, AtPIN1 normally accumulates in a highly polar manner in the root-ward (basal) plasma membranes of cambium (c) and xylem parenchyma (xp) vascular associated tissues (Bennett et al., 2016; Gälweiler et al., 1998). PIN1b accumulated in a similar pattern to AtPIN1 (Figure 2F, 2H. 10 samples from 5 events). In contrast, in addition to accumulating in the cambium and xylem parenchyma, SoPIN1 accumulated in the central pith tissue (p) (Figure 2E, 2G. 15 samples from 4 events). AtPIN1 is not normally observed in the pith (Bennett et al., 2016; Gälweiler et al., 1998). In the basal internode, both proteins showed the characteristic AtPIN1 root-ward polarization pattern regardless of tissue-level abundance (Figure 2K, 2M).

Taken together, these results show that even under the same transcriptional control SoPIN1 and PIN1b show distinct tissue-level accumulation patterns in Arabidopsis. While the overall behavior of the two Brachypodium proteins is similar to AtPIN1 in many tissues, there are behaviors unique to each. PIN1b fails to accumulate in the epidermal tissues where AtPIN1 and SoPIN1 remain high, whereas SoPIN1 accumulates in the pith tissue where AtPIN1 and PIN1b do not. The convergent polarization patterns of SoPIN1 and the vascular accumulation of PIN1b in Arabidopsis are remarkably similar to their native behaviors in Brachypodium

(O'Connor et al., 2014), suggesting conserved mechanisms might control tissue level abundance between the two species.

SoPIN1 but not PIN1b can restore organ initiation and bulk auxin transport in AtPIN1 null mutants

To determine whether the observed differences in SoPIN1 and PIN1b polarization and accumulation have functional consequences in Arabidopsis, we used the *proAtPIN1* driven SoPIN1 and PIN1b constructs to complement the Arabidopsis *pin1-613* mutant (also known as *pin1-7)*. The *pin1-613* allele is a putative null T-DNA insertion mutant with severe organ initiation defects in the inflorescence (Bennett et al., 2006; Smith et al., 2006; Zourelidou et al., 2014). Given that epidermal PIN1 function is important for organ initiation (Bilsborough et al., 2011; Kierzkowski et al., 2013), as expected only SoPIN1 was able to complement the *pin1-613* mutation and mediate organ initiation (Figure 3A) (3 out of 6 independent transgenic events showed complementation). However, phenotypic complementation of *pin1-613* by SoPIN1 was incomplete, and mature plants showed a variety of phenotypic defects (Figure 3A, Figure 3 - supplement 1). Most notably, each flower produced more sepals and petals than wild-type, but almost no stamens (Figure 3B, 3C, Figure 3 - supplement 2). SoPIN1 complemented *pin1-613* plants were thus sterile. We wondered if these phenotypes could be explained if SoPIN1 had poor auxin transport function in Arabidopsis. However, SoPIN1 restored wild-type levels of bulk auxin transport to *pin1-613* basal internodes (Figure 3D). Thus SoPIN1 is at least in part functionally capable of initiating organs and mediating root-ward auxin transport in the stem, but it is not functionally identical to AtPIN1 under the same promoter.

In SoPIN1 complemented *pin1-613* mutants, SoPIN1 accumulation increased in the meristem epidermis relative to wild-type or heterozygous plants, but the pronounced convergent polarization patterns observed in the WT background were less clear (Figure 4A, Figure 4 - supplement 1) (16 of 16 meristems). SoPIN1 complemented meristems showed a variety of phyllotactic defects and had highly variable morphologies (Figure 4 – supplement 1) (16 of 16 meristems). Similar to the pattern observed in the wild-type background, sub-epidermal SoPIN1 in *pin1-613* mutants accumulated in a loosely defined ring within which individual vein traces were difficult to discern (Figure 4I) (13 of 16 meristems). In the mature tissues, SoPIN1 accumulated in the epidermis, vasculature, and mature pith tissues similar to the wild-type background (Figure 4C, 4E, 4G).

In contrast to SoPIN1, PIN1b-expressing *pin1-613* plants had pin-formed inflorescences that were indistinguishable from *pin1-613* alone (Figure 3A) (all 7 events failed to complement). The lack of complementation mediated by PIN1b was not caused by silencing or low expression level because abundant PIN1b signal was observed in *pin1-613* meristems (23 of 26 *pin1-613* meristems from 7 events). In most PIN1b expressing *pin1-613* samples, expression increased in the epidermis relative to wildtype, forming a ring-shaped domain around the meristem apex (Figure 4B, 4D arrow, Figure 4 - supplement 2) (14 of 19 meristems from 6 events). Unlike in the wildtype background, PIN1b in the epidermis of *pin1-613* meristems was more consistently targeted to the membrane and polar (Figure 4K). However, even with this elevated polar expression in the meristem epidermis, PIN1b was unable to mediate organ initiation in *pin1-613*. Below the apex, PIN1b was polarized root-ward in *pin1-613* meristems (Figure 4J), forming defined traces associated with the vasculature (Figure 4F, 4L). In the basal stem of *pin1-613* mutants PIN1b accumulated in a pattern

similar to wild-type, although the arrangement of vascular bundles was irregular (Figure 4H). Remarkably, despite clear polar PIN1b expression in *pin1-613* mutant stems (Figure 4M), PIN1b was unable to rescue bulk auxin transport in this tissue (Figure 3D).

Although PIN1b was incapable of supporting organ formation or mediating bulk transport in *pin1-613,* when an auxin maximum was created artificially by addition of lanolin paste infused with IAA, PIN1b epidermal accumulation increased during the initiation of the resultant primordia (Figure 4 – supplement 3) (4 of 6 samples from 2 independent transgenic events). Thus, in the absence of AtPIN1, PIN1b accumulation in the epidermis is still auxin responsive and capable polar localization in *pin1-613* meristem tissue, but it is not able to mediate organ initiation itself. These results demonstrate that when expressed in *Arabidopsis,* there is a clear functional separation between SoPIN1 and PIN1b independent of transcriptional control.

SoPIN1 and PIN1b show different behaviors when expressed in the meristem epidermis

Epidermal-specific AtPIN1 expression is sufficient to rescue organ initiation in *atpin1* mutants (Bilsborough et al., 2011). In order to drive increased PIN1b expression in the epidermis, and to help reduce transgene position-effect variation of expression level, we utilized a two-component expression system in the Landsberg *erecta* (L*er*) background to drive SoPIN1 and PIN1b under the control of the epidermis-enriched Arabidopsis ML1 promoter (Hereafter designated *proAtML1>>*) (Lenhard, 2003; Sessions et al., 2002). Under the control of *proAtML1* we achieved consistently high epidermal accumulation of both SoPIN1 and PIN1b, but similar to the *proAtPIN1* driven

299 localization described above, only SoPIN1 showed clear convergent polarization
300 patterns around the sites of organ initiation (Figure 5A-5D, Figure 5 supplement 1 and
301 2) (11 of 11 meristems). Despite consistently high epidermal expression with this
302 system, PIN1b polarity remained difficult to determine, and in many cells the
303 abundance of protein on the membrane remained low (Figure 5D) (13 of 13
304 meristems). Instead, PIN1b accumulated in intracellular bodies, especially in the cells
305 of the apical dome and the central domain of initiating organs (Figure 5B, 5D arrow).
306 PIN1b abundance and polarity was highest at the boundaries of lateral organs (Figure
307 5 - supplement 2). Thus SoPIN1 and PIN1b show consistent behaviors in the meristem
308 epidermis when expressed under either *proAtPIN1* or *proAtML1.* However, despite
309 increased PIN1b expression under *proAtML1,* and a resulting increase in protein
310 accumulation in the apex, PIN1b was still unable to form convergent polarization
311 patterns in wildtype plants.

312

313 Both SoPIN1 and PIN1b can rescue the Arabidopsis *pin1-4* mutation
314 when expressed in the meristem epidermis

315 In order to determine whether the increased PIN1b abundance in the meristem
316 epidermis achieved by the *proAtML1* two-component system had functional
317 consequences, we crossed these transgenes into *pin1-4* mutant. The *pin1-4* allele is
318 in the Landsberg *erecta* background and has a single P579 to L amino acid change in
319 the second-to-last transmembrane domain of AtPIN1 (Bennett et al., 1995), but the
320 phenotype is similarly severe to *pin1-613* (Figure 6A). Remarkably, both SoPIN1 and
321 PIN1b driven by *proAtML1* were able to rescue the organ formation defects of *pin1-4*
322 (Figure 6A). In contrast to the SoPIN1-mediated complementation of *pin1-613*

described above, both SoPIN1 and PIN1b-complemented *pin1-4* plants made WT flowers that produced seed (Figure 6 – supplement 1). In addition, both *proAtML1* SoPIN1 and PIN1b expressing *pin1-4* lines were able to rescue bulk auxin transport in the basal internode, although PIN1b was less effective than SoPIN1 (Figure 6B). Compared to wildtype and SoPIN1-complemented plants, PIN1b-complemented *pin1-4* plants showed a significant increase in stem diameter (Figure 6C).

SoPIN1-complemented *pin1-4* meristems were slightly smaller than wildtype, and in rare cases showed defects in phyllotaxy (Figure 5 – supplement 1), but the protein localization was similar to the pattern observed in the WT background, with clear convergent polarization around initiating organs (Figure 5E, 5G) (10 of 10 meristems). In contrast, compared to the WT background, PIN1b localization in *pin1-4* was dramatically altered (Compare Figure 5B with Figure 5F). Most obvious was an increase in membrane targeted PIN1b and a corresponding reduction in intracellular PIN1b (Figure 5H). PIN1b polarity in the *pin1-4* background was more apparent than in wildtype, and convergent polarization patterns clearly marked incipient organs (Figure 5H) (10 of 10 meristems). PIN1b-complemented meristems accumulated less PIN protein in the apical dome compared to SoPIN1-complemented meristems, and the meristems were larger (Figure 5 – supplement 2).

In the basal internode, both PINs had similar accumulation patterns in the outer few cell layers (Figure 5I-J arrows), and both showed basal polarization in the epidermis (Figure 5K-L arrows). Despite this expression domain being drastically different than the wildtype vascular-associated pattern of AtPIN1 (Bennett et al., 2006; Gälweiler et al., 1998), expression in these few cortex layers and epidermis was apparently sufficient to drive wildtype levels of rootward bulk auxin transport in *pin1-4* (Figure 6B). Thus while both proteins can complement the *pin1-4* organ initiation phenotype, the

SoPIN1 and PIN1b complemented lines have differing localization patterns, slightly different auxin transport properties, and minor differences in meristem and mature plant morphologies, suggesting once again that SoPIN1 and PIN1b are not functionally identical.

Discussion

SoPIN1 and PIN1b have different functions in Brachypodium

During spikelet development in Brachypodium SoPIN1 forms convergent polarization patterns surrounding the sites of organ initiation and strong expression of the auxin response reporter DR5 (O'Connor et al., 2014). We provide additional evidence here that SoPIN1 polarizes towards sites of high auxin concentration by showing that a DII minimum occurs at SoPIN1 convergence points. In *sopin1* mutants the reduction of DII does not occur, suggesting that SoPIN1 functions to concentrate auxin at epidermal maxima, and similar to *Arabidopsis,* this is required for organ initiation in the inflorescence. The specificity of SoPIN1 for the outer tissues in Brachypodium provides further support for the idea that maxima formation is necessary for organ initiation, and that this is primarily mediated by convergent PIN in the meristem epidermis (Bhatia et al., 2016; Jönsson et al., 2006; Kierzkowski et al., 2013; Smith et al., 2006).

SoPIN1 clade mutants have been reported in the legume *Medicago truncatula* and in tomato (*Solanum lycopersicum*), and these mutants show pleiotropic phenotypes involving phyllotaxy, organ initiation, inflorescence branching, leaf serrations, and leaf compounding, but they do not form barren pin meristems (Martinez et al., 2016; Zhou

et al., 2011). These wider morphogenetic events also involve epidermal PIN convergence points and associated auxin maxima, suggesting a general role for SoPIN1 clade members in generating such maxima (Barkoulas et al., 2008; Bilsborough et al., 2011). But the lack of barren pin-formed meristems in these mutants may suggest that different species are variably dependent on SoPIN1-generated maxima for organ initiation.

In contrast to *sopin1*, loss of PIN1b function has no clear organ initiation defects, despite being expressed in developing organs (O'Connor et al., 2014). Given that auxin drainage is thought necessary for proper organ size and placement (Bhatia et al., 2016; Deb et al., 2015), the lack of an organ initiation phenotype in *pin1b* is surprising. However, it is possible that PIN1a performs some of this function, and double mutants are needed to address the redundancy of PIN1a and PIN1b during organ initiation.

The increased internode elongation in *pin1b* mutants provides new genetic tractability to address how PINs regulate tissue growth in the shoot independent of organ initiation. Grasses contain intercalary meristems, bands of indeterminate tissue separated from the apical meristem that are responsible for internode growth after organ initiation. PIN1b expression around this meristematic tissue (Figure 1I) suggests that PIN1b may regulate growth by influencing auxin distribution in this meristem. This is consistent with evidence that loss of the ABCB1 auxin exporter in maize results in dwarfism associated with reduced activity of intercalary meristems (Knöller et al., 2010). How PIN1b alters auxin dynamics to control internode growth will be an important direction for future research.

The properties that define PIN behavior and function

Membrane accumulation. Because of their differing phenotypes in Brachypodium, we used heterologous expression of SoPIN1 and PIN1b in Arabidopsis to explore the ways in which different PIN family members may have different properties post-transcription (Summarized in Figure 7). When expressed in the meristem epidermis in wild-type Arabidopsis, SoPIN1 is localized to the membrane in most cells while PIN1b often accumulates internally (Compare Figure 5C and D). Thus, with the same transcriptional control different PINs can vary in the degree to which, after protein production, they accumulate at the plasma membrane. The differential membrane targeting of PIN1b and SoPIN1 is a tissue-specific phenomenon however, because unlike in the epidermis, in the basal internode both PINs accumulate at the plasma membrane (Figure 2K, 2M). The regulation of PIN plasma membrane polar targeting and endocytic recycling has been an important avenue for understanding PIN function and general membrane protein biology (Luschnig and Vert, 2014). Our results provide further evidence that at least some of the signals governing membrane accumulation are inherent in, and vary between different PIN family members.

Tissue accumulation. Under the same transcriptional control SoPIN1 and PIN1b show different tissue-level accumulation patterns in Arabidopsis. In wildtype plants *proAtPIN1*-expressed PIN1b shows less overall accumulation in the epidermis compared to SoPIN1 (Compare Figure 2C and 2D). The punctate PIN1b signal in the meristem epidermis may be PIN1b protein being actively targeted for degradation as has been shown for PIN2 in the root (Abas et al., 2006). In contrast, SoPIN1 is abundant in the epidermis and accumulates in an expanded expression domain in the sub-epidermal meristem tissues (Compare Figure 2J and 2L). Also, in the basal

internode SoPIN1 accumulates in the pith tissue where AtPIN1 and PIN1b do not (Figure 2E, 2G). The presence of SoPIN1 in the pith is not easy to explain because AtPIN1 shows no protein accumulation in this tissue. It is possible however that the sub-epidermal SoPIN1 protein accumulation in the meristem persists into the mature internode.

In Arabidopsis, endogenous PIN family members show a degree of cross-regulation where loss-of-function mutations in one PIN family member result in ectopic accumulation of a different PIN in a compensatory pattern (Blilou et al., 2005; Paponov et al., 2005; Vieten et al., 2005). We observed similar behavior in the *pin1-613* null background where SoPIN1 and PIN1b accumulation in the meristem epidermis was increased in the absence of AtPIN1 (Figure 4 supplements 1 and 2). However, we did not observe the same cross-regulation in the *pin1-4* background where SoPIN1 and PIN1b tissue-level accumulation seemed similar between *pin1-4* mutant and wild-type meristems (Figure 5 - supplements 1 and 2). These variable tissue-level abundances, and PIN cross-regulation behaviors highlight the overall redundancy of some PIN behaviors, and further demonstrate the importance of PIN post-transcriptional regulation for controlling PIN abundance.

Transport activity. In Arabidopsis, phosphorylation of PINs by several different families of protein kinases is necessary for efficient auxin transport (Barbosa et al., 2014; Jia et al., 2016; Willige et al., 2013; Zourelidou et al., 2014). The necessity for PIN activation by phosphorylation may explain the inability of PIN1b to mediate bulk auxin transport in the basal internode of *pin1-613* plants despite being expressed, accumulating at the membrane, and being polarized root-ward in this tissue (Figure 4M). It is possible that in the *proAtPIN1* domain PIN1b does not interact with the appropriate activating kinase, and it is thus inactive. Indeed, a partially un-

444 phosphorylatable form of AtPIN1 fails to complement fully the bulk auxin transport
445 defect of *pin1-613* mutants in the basal internode (Zourelidou et al., 2014). However,
446 when expressed using *proAtML1,* PIN1b expression in the outer tissue layers of the
447 basal internode appears sufficient to mediate bulk auxin transport in *pin1-4* (Figure
448 6B), suggesting that PIN1b activity may be tissue dependent, perhaps because of the
449 differing expression domains of activating kinases (Zourelidou et al., 2014). Indeed,
450 Arabidopsis PIN4 and PIN7 are present in the *proAtML1* domain (Bennett et al., 2016),
451 making it conceivable that these PINs are the normal targets of activating kinases in
452 this tissue. Regardless, the behavior of PIN1b in *pin1-613* Arabidopsis provides a clear
453 indication that even once a PIN has accumulated at the cell membrane in a tissue it
454 may not be active.

455 **Interaction.** A particularly striking result is the ability of PIN1b to form convergent
456 polarization patterns and mediate organ initiation in the *pin1-4* missense mutant
457 background when it is unable to do so in the null *pin1-613* background. The strong
458 influence of *pin1-4* on PIN1b membrane targeting and polarity in the meristem
459 epidermis (Compare Figures 6D and 6H) suggests that PIN1b may be cooperating
460 with a partially functional *pin1-4* protein and together they recapitulate the functions of
461 wildtype AtPIN1. The presence of some *pin1-4* function is supported by the result that
462 SoPIN1 complementation of the null *pin1-613* allele is partial, and because of flower
463 defects the plants are sterile (Figure 3B, 3C), while complementation of *pin1-4* is
464 complete and flowers are phenotypically normal and set seed (Figure 6 - supplement
465 1). Consistent with these different complementation phenotypes, SoPIN1 convergent
466 patterns are more evident in the presence of *pin1-4* than they are in the null *pin1-613*
467 background (Compare 4A and 5E), further evidence for partial *pin1-4* function. If PIN1b
468 is indeed inactive in null *pin1-613* mutants as we hypothesized above, then it is

469 possible *pin1-4* facilitates the interaction of PIN1b with the appropriate activating
470 kinase, and this allows PIN1b to perform organ initiation. Alternatively, *pin1-4* may
471 provide polarity information that PIN1b lacks, and even though *pin1-4* is non-
472 functional, it is able to target or stabilize PIN1b on the appropriate membrane to
473 mediate convergent polarization patterns and organ initiation. However, *pin1-4*
474 interaction with PIN1b cannot explain the ability of PIN1b to rescue bulk transport in
475 the basal internodes of *pin1-4* mutants, because the two proteins presumably do not
476 overlap in this tissue. In this case the necessary interaction between PIN1b and *pin1-*
477 *4* may be set up early during organ initiation, and protein modifications propagated to
478 the basal internode. Direct PIN interaction has so far never been shown, but if one PIN
479 type can convey polarity or activity information to another through direct interaction
480 this may be important for understanding auxin transport in tissues where multiple PINs
481 overlap, such as in the root meristem (Blilou et al., 2005), or in Brachypodium where
482 multiple PINs are present during organ initiation in the shoot (O'Connor et al., 2014).

483 **Polarity.** We previously showed that the polarization dynamics of SoPIN1, PIN1a, and
484 PIN1b in *Brachypodium* could be modeled by assigning two different polarization
485 modes to the SoPIN1 and PIN1 clades (O'Connor et al., 2014). In the model, SoPIN1
486 orients toward the adjacent cell with the highest auxin concentration, thus transporting
487 auxin up the concentration gradient and providing a positive feedback to concentrate
488 auxin into local maxima. In contrast, in the model PIN1a and PIN1b proteins are
489 allocated in proportion to auxin flux, thus providing a positive feedback where flux
490 through the tissue is amplified by the allocation of PIN1a/b in the direction of that flux.
491 The assignment of two different polarization modes was previously used to describe
492 the behavior of AtPIN1 during organ placement and vein patterning utilizing an auxin-
493 concentration based switching mechanism between the up-the-gradient (UTG) and

494 with-the-flux (WTF) polarization modes (Bayer et al., 2009). However, it has also been
495 suggested that a flux-based mechanism alone can account for both convergence
496 points and vein patterning (Abley et al., 2016; Stoma et al., 2008).

497 Despite evidence that PIN polarization is dependent on localized auxin signaling
498 (Bhatia et al., 2016), there are still no known mechanisms for direct sensing of
499 intercellular auxin gradients or flux across membranes. However, the *sopin1* and *pin1b*
500 phenotypes in Brachypodium are consistent with different polarization modes. SoPIN1
501 is required for organ initiation and the formation of auxin maxima in Brachypodium,
502 which is primarily modeled using UTG polarization (Bayer et al., 2009; Jönsson et al.,
503 2006; Smith et al., 2006). On the other hand, *pin1b* mutant plants do not show organ
504 initiation defects, but rather only have internode elongation defects, a tissue where
505 WTF models have been used to explain PIN dynamics and measured auxin transport
506 kinetics during vein patterning and the regulation of branch outgrowth (Bayer et al.,
507 2009; Bennett et al., 2016; Mitchison, 1980; Mitchison et al., 1981; Prusinkiewicz et
508 al., 2009).

509 In wild-type Brachypodium the SoPIN1 and PIN1b expression domains are almost
510 entirely mutually exclusive (O'Connor et al., 2014), making it possible that the
511 observed polarization differences between the two clades are due to expression
512 context and not functional differences between the proteins themselves. More
513 specifically, perhaps an UTG mechanism dominates the epidermis while a WTF
514 mechanism is utilized in the internal tissues, and different PINs interact equally with
515 these context-dependent mechanisms. Our heterologous expression studies do not
516 exclusively support context-dependent or protein-dependent mechanisms for SoPIN1
517 and PIN1b polarity. It is clear that alone only SoPIN1 and AtPIN1 show the convergent
518 polarization patterns associated with UTG polarization, and alone only SoPIN1 and

519 AtPIN1 are thus able to mediate organ initiation, while PIN1b cannot. On the other
520 hand, all three PINs are capable of root-ward polarization in the basal internode tissue.
521 The results presented here do not demonstrate whether within a single cell PIN1b and
522 SoPIN1 would orient differently with respect to auxin as might be expected for the dual
523 polarization model (O'Connor et al., 2014). However such context-independent
524 polarization behavior was previously observed for PIN1 and PIN2 in the root where
525 both PINs can polarize in opposing directions within a single cell type when expressed
526 in the PIN2 domain (Kleine-Vehn et al., 2008; Wisniewska et al., 2006).

527 ## Outlook

528 In total, our Brachypodium mutant phenotypes and heterologous expression results
529 point to multiple levels at which PIN family members can be functionally distinct.
530 Differential membrane targeting, tissue level accumulation, transport activity, indirect
531 or direct interaction, and the resultant polarity may all contribute to the dynamics of
532 PIN action during plant development. In most flowering plants two PIN clades, SoPIN1
533 and PIN1, with differing properties post-transcription mediate auxin transport in the
534 shoot, but these properties are seemingly combined into AtPIN1 in Arabidopsis and
535 other Brassicaceae species. Because PIN1b is unable to mediate organ initiation while
536 AtPIN1 can, and these two PINs are both members of the same clade, AtPIN1 may
537 have gained the ability to form convergent polarization patterns and mediate organ
538 initiation after, or coincident with, the loss of the SoPIN1 clade. Indeed, when
539 comparing Brassicaceae PIN1 proteins against a broad sampling of other angiosperm
540 PIN1 proteins, the Brassicaceae PIN1 proteins have several divergent protein
541 domains (Figure 7 - supplement 1), suggesting possible neofunctionalization within
542 the Brassicacea family. Alternatively, an expansion of the PIN3,4,7 clade is also

543 characteristic of Brassicacea species (Bennett et al., 2014; O'Connor et al., 2014),
544 making it possible duplicated members of this clade buffered the loss of SoPIN1.
545 However, there is no indication that PIN3,4,7 have a role in organ initiation in the
546 inflorescence (Guenot et al., 2012). Regardless, we believe the combination of
547 SoPIN1 and PIN1 characteristics into AtPIN1 coincident with the loss of the SoPIN1
548 clade represents a form of reverse-subfunctionalization, the combination of functions
549 originally split between homologs into a single protein after gene loss. It is not
550 surprising that PINs may be particularly amenable to this kind of functional evolution
551 because, as described above, there are several post-transcriptional regulatory steps
552 that ultimately combine to control PIN function in plants. The output of auxin transport
553 is the sum of a vast network of post-transcriptional interactions that all act to regulate
554 auxin transport itself, and this gives the system plasticity during development, and
555 perhaps also over evolutionary time.

556

557 Materials and Methods

558 *sopin1-1* and *pin1b-1* creation with CRISPR

559 SoPIN1 (Bradi4g26300) and PIN1b (Bradi3g59520) were targeted with CRISPR using
560 vectors developed for rice (Miao et al., 2013). CRISPR constructs were transformed
561 into Brachypodium inbred line Bd21-3 using previously published methods (Bragg et
562 al., 2015).

563 *sopin1-1* CRISPR

564 The SoPIN1 guide was AGGCTGTCGTACGAGGAGT. This guide was shorter than
565 the typical 20bp in an effort to provide greater target specificity for SoPIN1 (Fu et al.,

2014). In the T0 regenerated plants, 5 out of 9 independent transgenic events showed severe organ initiation defects, and all 5 contained lesions in the SoPIN1 CRIPSR target site. Unfortunately, only one of the events with a T0 phenotype set seed. In the T1 progeny of this event only those individuals that contained the CRISPR transgene showed lesions in the SoPIN1 CRISPR target site, and these plants showed the *sopin1* phenotype and thus failed to set seed, suggesting active editing by the SoPIN1 CRISPR transgene in this event.

Not all events showed such efficient editing however, and we identified an independent T1 family where a C insertion in the SoPIN1 CRISPR target site co-segregated with the barren inflorescence phenotype. We designated this allele, which causes a premature stop codon before the end of the third exon codon 739 base pairs downstream from the target site, *sopin1-1*. We backcrossed a heterozygous *sopin1-1* plant to the Bd21-3 parental line and all F1 progeny (N=4) were wildtype. In the F2 generation, the *sopin1-1* lesion co-segregated with the barren inflorescence phenotype (N=60: 32 het, 18 homo,10 wt). Amongst these plants, 16 did not have the Cas9 transgene, and the barren inflorescence phenotype still co-segregated with the *sopin1-1* lesion (N=16: 8 het, 3 homo, 5 wt). We crossed the T1 *sopin1-1* heterozygous plant with a line homozygous for the SoPIN1-Citrine genomic reporter line (O'Connor et al., 2014). In the F2 we identified families homozygous for *sopin1-1* but segregating for the SoPIN1-Citrine transgene. Only individuals that lacked the SoPIN1-Citrine transgene showed a *sopin1-1* phenotype, while those that contained the SoPIN1-Citrine transgene made spikelets and set seed. This complementation was independent of the presence of Cas9.

pin1b-1 CRISPR

The PIN1b guide was AGGGCAAGTACCAGATCC. We identified a single plant from the regenerating T0 PIN1b CRISPR population that had longer basal internodes and twisted leaves. This plant was homozygous for an A deletion in the PIN1b CRISPR target site causing a premature stop in the second exon 502 base pairs downstream, here designated *pin1b-1*. All T1 progeny showed the *pin1b* phenotype and were homozygous for the *pin1b-1* lesion. We backcrossed these T1 plants to Bd21-3 and all F1 progeny had a wild-type phenotype (N=11). In the F2, the *pin1b* phenotype co-segregated with the *pin1b-1* lesion (N= 215, 91 het, 39 homo, 26 wt). Amongst these plants, 24 did not have the Cas9 transgene, and the *pin1b* phenotype co-segregated perfectly with the *pin1b-1* lesion (N=24: 10 het, 6 homo, 8 wt).

Brachypodium Reporter Constructs

All constructs were cloned using Multi-site Gateway (Invitrogen) and were transformed into Brachypodium Bd21-3 using previously published methods (Bragg et al., 2015). For pZmUbi::DII-Venus, we first cloned the maize ubiquitin promoter into pDONR P4-P1R (Primer IDs 1-2 Table 1) and this was subsequently recombined with pDONR 221 containing Arabidopsis DII and pDONR P2R-P3 containing VENUS-N7 (Brunoud et al., 2012) into the Multi-site Gateway binary vector pH7m34GW (http://gateway.psb.ugent.be/). In the T3 generation, degradation of DII-Venus in the presence of auxin was validated by treating excised Brachypodium spikelet meristems with 1 µM 1-naphthaleneacetic acid (NAA) or mock treatment in 70% ethanol, and imaging every 30 min (Figure 1 – figure supplement 2).

For SoPIN1-Cerulean, the promoter plus 5' coding pDONR-P4-P1R and 3' coding plus downstream pDONR-P2R-P3 fragments from (O'Connor et al., 2014) were used. Maize codon-optimized Cerulean florescent protein, courtesy of David Jackson, was

amplified with 5x Ala linkers and cloned into pENTR/D-TOPO. These three fragments were then recombined into pH7m34GW.

Arabidopsis Reporter Constructs

All constructs were cloned using Multi-site Gateway (Invitrogen) and transformed using standard floral dip. For *proAtPIN1* complementation, a 3.5kb Arabidopsis PIN1 promoter region was amplified from a genomic clone previously reported to complement the *pin1* (Heisler et al., 2005) and cloned into Gateway vector pDONR P4-P1R (Primer IDs 3-4 Table 1). For each Brachypodium PIN-Citrine fusion construct, the entire PIN coding region, including the Citrine insertion, was amplified from the previously published reporter constructs (O'Connor et al., 2014) and cloned into pENTR /D-TOPO (Primer IDs 5-8 Table 1). The *proAtPIN1* pDONR P4-P1R and PIN coding region pENTR/D-TOPO vectors were then recombined into Gateway binary vector pH7m24GW (http://gateway.psb.ugent.be/) and transformed by floral dip into both Col-0 and plants heterozygous for *pin1-613* (also known as *pin1-7,* SALK_047613) (Bennett et al., 2006; Smith et al., 2006). Complementation was assessed in the T3 generation, and all plants were genotyped for both the *pin1-613* mutation (Primer IDs 9-11 Table 1) and for presence of the PIN transgene (Primer IDs 12-14 Table 1).

For the *proAtML1* lines the PIN coding regions with Citrine insertion pENTR /D-TOPO Gateway vectors were recombined downstream of the two-component OP promoter in vector pMoA34-OP (Moore et al., 1998) and then transformed into the *proAtML1* driver line in the Landsberg *erecta* background (Lenhard, 2003). Lines homozygous for both the *proAtML1* driver and OP::PIN were crossed to het *pin1-4* and complementation was assessed in the F2 and F3 generations. All complemented

638 plants were genotyped for *pin1-4* (Primer IDs 15-16 Table 1 with AciI digestion), the
639 Brachypodium PINs (Primer IDs 12-14 Table 1), and the presence of the ML1 driver
640 transgene (Primer IDs 17-18 Table 1).

641 ## Confocal Imaging

642 All confocal images were captured on a Zeiss 780 laser scanning confocal using
643 514nm excitation and a W Plan-Apochromat 20x magnification 1.0 numerical aperture
644 objective. Detection wavelengths: 517-570nm for Citrine tagged PINs, 631-717nm for
645 Propidium Iodide, and 646-726 for chlorophyll A auto-fluorescence. The pinhole was
646 set to 1 airy unit for all meristem stacks and details of sub-epidermal polarization, but
647 was open to the maximum setting for tiled longitudinal and cross sections of the basal
648 internode (Figures 2C-H, 4C-H and 5I-J). Detection gain and laser power were varied
649 according to signal strength unless direct comparisons between genotypes were made
650 as indicated in figure legends.

651 ## Auxin Transport Assays

652 Auxin transport assays were carried out as described in (Crawford et al., 2010). Briefly,
653 17 mm long basal internodes were excised and the apical end submerged in 30 µl
654 Arabidopsis salts (ATS) without sucrose (pH = 5.6) containing 1 µM ^{14}C-IAA (American
655 Radiolabeled Chemicals). After 6 hours incubation, the basal 5 mm segment was
656 excised, cut in half, and shaken overnight at 400 RPM in 200 µl scintillation liquid prior
657 to scintillation counting. 10µM N-1-Naphthylphthalamic Acid (NPA), an auxin transport
658 inhibitor, was added prior to incubation for negative controls.

659

Acknowledgments

Thanks to Fabrizio Ticchiarelli for genotyping help, Martin van Rongen for assistance with transport assays and *pin1-613* oligos, Tom Bennett for *proAtPIN1* oligos, Marcus Heisler for AtPIN1-GFP construct and *pin1-4* genotyping assistance, Teva Vernoux for DII plasmids, David Jackson for maize codon-optimized Cerulean, and to all the members of the Leyser lab. Thanks also to Graeme Mitchison, Katie Abley and Pau Formosa-Jordan for helpful comments on the manuscript.

References

Abas, L., Benjamins, R., Malenica, N., Paciorek, T., Wisniewska, J., Wirniewska, J., Moulinier-Anzola, J. C., Sieberer, T., Friml, J. and Luschnig, C. (2006). Intracellular trafficking and proteolysis of the Arabidopsis auxin-efflux facilitator PIN2 are involved in root gravitropism. *Nat Cell Biol* **8**, 249–256.

Abley, K., Marée, A. F. and Coen, E. (2016). Formation of polarity convergences underlying shoot outgrowths. *eLife* **5**, 2061.

Adamowski, M. and Friml, J. (2015). PIN-Dependent Auxin Transport: Action, Regulation, and Evolution. *The Plant Cell* **27**, 20–32.

Barbosa, I. C. R., Zourelidou, M., Willige, B. C., Weller, B. and Schwechheimer, C. (2014). D6 PROTEIN KINASE activates auxin transport-dependent growth and PIN-FORMED phosphorylation at the plasma membrane. *Dev Cell* **29**, 674–685.

Barkoulas, M., Hay, A., Kougioumoutzi, E. and Tsiantis, M. (2008). A developmental framework for dissected leaf formation in the Arabidopsis relative Cardamine hirsuta. *Nat Genet* **40**, 1136–1141.

Bayer, E. M., Bayer, E. M., Smith, R. S., Mandel, T., Nakayama, N., Sauer, M., Prusinkiewicz, P. and Kuhlemeier, C. (2009). Integration of transport-based models for phyllotaxis and midvein formation. *Genes Dev* **23**, 373–384.

Benková, E., Michniewicz, M., Sauer, M., Teichmann, T., Seifertová, D., Jürgens, G. and Friml, J. (2003). Local, Efflux-Dependent Auxin Gradients as a Common Module for Plant Organ Formation. *Cell* **115**, 591–602.

Bennett, S. R. M., Alvarez, J., Bossinger, G. and Smyth, D. R. (1995). Morphogenesis in pinoid mutants of Arabidopsis thaliana. *Plant J* **8**, 505–520.

Bennett, T. A., Brockington, S. F., Rothfels, C., Graham, S. W., Stevenson, D., Kutchan, T., Rolf, M., Thomas, P., Wong, G. K.-S., Leyser, H. M. O., et al. (2014). Paralogous radiations of PIN proteins with multiple origins of noncanonical PIN structure. *Molecular Biology and Evolution* **31**, 2042–2060.

Bennett, T. A., Hines, G., van Rongen, M., Waldie, T., Sawchuk, M. G., Scarpella, E., Ljung, K. and Leyser, H. M. O. (2016). Connective Auxin Transport in the Shoot Facilitates Communication between Shoot Apices. *PLoS Biol* **14**, e1002446.

Bennett, T. A., Sieberer, T., Willett, B., Booker, J., Luschnig, C. and Leyser, H. M. O. (2006). The Arabidopsis MAX Pathway Controls Shoot Branching by Regulating Auxin Transport. *Current Biology* **16**, 553–563.

Bhatia, N., Bozorg, B., Larsson, A., Ohno, C., Jönsson, H. and Heisler, M. G. (2016). Auxin Acts through MONOPTEROS to Regulate Plant Cell Polarity and Pattern Phyllotaxis. *Curr Biol* **26**, 3202–3208.

Bilsborough, G. D., Runions, A., Barkoulas, M., Jenkins, H. W., Hasson, A., Galinha, C., Laufs, P., Hay, A., Prusinkiewicz, P. and Tsiantis, M. (2011). Model for the regulation of Arabidopsis thaliana leaf margin development. *Proc Natl Acad Sci USA* **108**, 3424–3429.

Blilou, I., Xu, J., Wildwater, M., Willemsen, V., Paponov, I., Friml, J., Heidstra, R., Aida, M., Palme, K. and Scheres, B. (2005). The PIN auxin efflux facilitator network controls growth and patterning in Arabidopsis roots. *Nature* **433**, 39–44.

Bragg, J. N., Anderton, A., Nieu, R. and Vogel, J. P. (2015). Brachypodium distachyon. *Methods Mol Biol* **1223**, 17–33.

Brunoud, G., Wells, D. M., Oliva, M., Larrieu, A., Mirabet, V., Burrow, A. H., Beeckman, T., Kepinski, S., Traas, J., Bennett, M. J., et al. (2012). A novel sensor to map auxin response and distribution at high spatio-temporal resolution. *Nature* **482**, 103–106.

Crawford, S., Shinohara, N., Sieberer, T., Williamson, L., George, G., Hepworth, J., Muller, D., Domagalska, M. A. and Leyser, H. M. O. (2010). Strigolactones enhance competition between shoot branches by dampening auxin transport. *Development* **137**, 2905–2913.

Deb, Y., Marti, D., Frenz, M., Kuhlemeier, C. and Reinhardt, D. (2015). Phyllotaxis involves auxin drainage through leaf primordia. *Development* **142**, dev.121244–2001.

Fu, Y., Sander, J. D., Reyon, D., Cascio, V. M. and Joung, J. K. (2014). Improving CRISPR-Cas nuclease specificity using truncated guide RNAs. *Nat Biotechnol* **32**, 279–284.

Gälweiler, L., Guan, C., Müller, A., Wisman, E., Mendgen, K., Yephremov, A. and Palme, K. (1998). Regulation of Polar Auxin Transport by AtPIN1 in Arabidopsis Vascular Tissue. *Science* **282**, 2226–2230.

Gordon, S. P., Heisler, M. G., Reddy, G. V., Ohno, C., Das, P. and Meyerowitz, E. M. (2007). Pattern formation during de novo assembly of the Arabidopsis shoot meristem. *Development* **134**, 3539–3548.

Guenot, B., Bayer, E. M., Bayer, E., Kierzkowski, D., Smith, R. S., Mandel,

T., Zádníková, P., Benková, E. and Kuhlemeier, C. (2012). Pin1-independent leaf initiation in Arabidopsis. *Plant Physiol* **159**, 1501–1510.

Habets, M. E. J. and Offringa, R. (2014). PIN-driven polar auxin transport in plant developmental plasticity: a key target for environmental and endogenous signals. *New Phytologist* **203**, 362–377.

Heisler, M. G., Hamant, O., Krupinski, P., Uyttewaal, M., Ohno, C., Jönsson, H., Traas, J. and Meyerowitz, E. M. (2010). Alignment between PIN1 polarity and microtubule orientation in the shoot apical meristem reveals a tight coupling between morphogenesis and auxin transport. *PLoS Biol* **8**, e1000516.

Heisler, M. G., Ohno, C., Das, P., Sieber, P., Reddy, G. V., Long, J. A. and Meyerowitz, E. M. (2005). Patterns of auxin transport and gene expression during primordium development revealed by live imaging of the Arabidopsis inflorescence meristem. *Curr Biol* **15**, 1899–1911.

Jia, W., Li, B., Li, S., Liang, Y., Wu, X., Ma, M., Wang, J., Gao, J., Cai, Y., Zhang, Y., et al. (2016). Mitogen-Activated Protein Kinase Cascade MKK7-MPK6 Plays Important Roles in Plant Development and Regulates Shoot Branching by Phosphorylating PIN1 in Arabidopsis. *PLoS Biol* **14**, e1002550.

Jönsson, H., Heisler, M. G., Shapiro, B. E., Meyerowitz, E. M. and Mjolsness, E. (2006). An auxin-driven polarized transport model for phyllotaxis. *Proc Natl Acad Sci USA* **103**, 1633–1638.

Kierzkowski, D., Lenhard, M., Smith, R. S. and Kuhlemeier, C. (2013). Interaction between meristem tissue layers controls phyllotaxis. *Dev Cell* **26**, 616–628.

Kleine-Vehn, J., Dhonukshe, P., Sauer, M., Brewer, P. B., Wisniewska, J., Paciorek, T., Benková, E. and Friml, J. (2008). ARF GEF-dependent transcytosis and polar delivery of PIN auxin carriers in Arabidopsis. *Curr Biol* **18**, 526–531.

Knöller, A. S., Blakeslee, J. J., Richards, E. L., Peer, W. A. and Murphy, A. S. (2010). Brachytic2/ZmABCB1 functions in IAA export from intercalary meristems. *J Exp Bot* **61**, 3689–3696.

Lenhard, M. (2003). Stem cell homeostasis in the Arabidopsis shoot meristem is regulated by intercellular movement of CLAVATA3 and its sequestration by CLAVATA1. *Development* **130**, 3163–3173.

Leyser, H. M. O. (2005). Auxin Distribution and Plant Pattern Formation: How Many Angels Can Dance on the Point of PIN? *Cell* **121**, 819–822.

779 **Leyser, H. M. O.** (2006). Dynamic integration of auxin transport and
780 signalling. *CURBIO* **16**, R424–33.

781 **Leyser, H. M. O.** (2010). The power of auxin in plants. *Plant Physiol* **154**,
782 501–505.

783 **Luschnig, C. and Vert, G.** (2014). The dynamics of plant plasma membrane
784 proteins: PINs and beyond. *Development* **141**, 2924–2938.

785 **Martinez, C. C., Koenig, D., Chitwood, D. H. and Sinha, N. R.** (2016). A
786 sister of PIN1 gene in tomato (Solanum lycopersicum) defines leaf and
787 flower organ initiation patterns by maintaining epidermal auxin flux. *Dev*
788 *Biol* **419**, 85–98.

789 **Miao, J., Guo, D., Zhang, J., Huang, Q., Qin, G., Zhang, X., Wan, J., Gu, H.**
790 **and Qu, L.-J.** (2013). Targeted mutagenesis in rice using CRISPR-Cas
791 system. *Cell Res* **23**, 1233–1236.

792 **Mitchison, G. J.** (1980). A Model for Vein Formation in Higher Plants. *Proc.*
793 *Biol. Sci.* **207**, 79–109.

794 **Mitchison, G. J., Hanke, D. E. and Sheldrake, A. R.** (1981). The Polar
795 Transport of Auxin and Vein Patterns in Plants [and Discussion].
796 *Philosophical Transactions of the Royal Society B: Biological Sciences*
797 **295**, 461–471.

798 **Moore, I., Gälweiler, L., Grosskopf, D. and Palme, K.** (1998). A transcription
799 activation system for regulated gene expression in transgenic plants. *Proc.*
800 *Natl. Acad. Sci. U.S.A.* **95**, 376–381.

801 **O'Connor, D. L., Runions, A., Runions, A., Sluis, A., Sluis, A., Bragg, J.,**
802 **Bragg, J., Vogel, J. P., Vogel, J. P., Prusinkiewicz, P., et al.** (2014). A
803 division in PIN-mediated auxin patterning during organ initiation in grasses.
804 **10**, e1003447.

805 **Okada, K., Ueda, J., Komaki, M. K., Bell, C. J. and Shimura, Y.** (1991).
806 Requirement of the Auxin Polar Transport System in Early Stages of
807 Arabidopsis Floral Bud Formation. *The Plant Cell* **3**, 677–684.

808 **Paponov, I. A., Teale, W. D. and Trebar, M.** (2005). The PIN auxin efflux
809 facilitators: evolutionary and functional perspectives. *Trends Plant Sci* **10**,
810 170–177.

811 **Prusinkiewicz, P., Crawford, S., Smith, R. S., Ljung, K., Bennett, T. A.,**
812 **Ongaro, V. and Leyser, H. M. O.** (2009). Control of bud activation by an
813 auxin transport switch. *Proc Natl Acad Sci USA* **106**, 17431–17436.

814 **Raven, J. A.** (1975). Transport of indoleacetic acid in plant cells in relation to
815 pH and electrical potential gradients, and its significance for polar IAA

816 transport. *New Phytol* **74**, 163–172.

817 **Reinhardt, D., Mandel, T. and Kuhlemeier, C.** (2000). Auxin Regulates the
818 Initiation and Radial Position of Plant Lateral Organs. *The Plant Cell* **12**,
819 507.

820 **Reinhardt, D., Pesce, E.-R., Stieger, P., Mandel, T., Baltensperger, K.,**
821 **Bennett, M. J., Traas, J., Friml, J. and Kuhlemeier, C.** (2003).
822 Regulation of phyllotaxis by polar auxin transport. *Nature* **426**, 255–260.

823 **Rubery, P. H. and Sheldrake, A. R.** (1974). Carrier-mediated auxin transport.
824 *Planta* **118**, 101–121.

825 **Sawchuk, M. G., Edgar, A. and Scarpella, E.** (2013). Patterning of Leaf Vein
826 Networks by Convergent Auxin Transport Pathways. *PLoS Genet* **9**,
827 e1003294.

828 **Scarpella, E., Marcos, D., Friml, J. and Berleth, T.** (2006). Control of leaf
829 vascular patterning by polar auxin transport. *Genes Dev* **20**, 1015–1027.

830 **Sessions, A., Weigel, D. and Yanofsky, M. F.** (2002). The Arabidopsis
831 thaliana MERISTEM LAYER 1 promoter specifies epidermal expression in
832 meristems and young primordia. *Plant J* **20**, 259–263.

833 **Shinohara, N., Taylor, C. and Leyser, H. M. O.** (2013). Strigolactone Can
834 Promote or Inhibit Shoot Branching by Triggering Rapid Depletion of the
835 Auxin Efflux Protein PIN1 from the Plasma Membrane. *PLoS Biol* **11**,
836 e1001474.

837 **Smith, R. S., Guyomarc'h, S., Mandel, T., Reinhardt, D., Kuhlemeier, C.**
838 **and Prusinkiewicz, P.** (2006). A plausible model of phyllotaxis. *Proc. Natl.*
839 *Acad. Sci. U.S.A.* **103**, 1301–1306.

840 **Stoma, S., Lucas, M., Chopard, J., Schaedel, M. and Godin, C.** (2008).
841 Flux-Based Transport Enhancement as a Plausible Unifying Mechanism
842 for Auxin Transport in Meristem Development. *PLoS Comput Biol* **4**,
843 e1000207.

844 **Verna, C., Sawchuk, M. G., Linh, N. M. and Scarpella, E.** (2015). Control of
845 vein network topology by auxin transport. *BMC Biol* **13**, 94.

846 **Vieten, A., Vanneste, S., Wisniewska, J., Benkova, E., Benjamins, R.,**
847 **Beeckman, T., Luschnig, C. and Friml, J.** (2005). Functional redundancy
848 of PIN proteins is accompanied by auxin-dependent cross-regulation of
849 PIN expression. *Development* **132**, 4521–4531.

850 **Willige, B. C., Ahlers, S., Zourelidou, M., Barbosa, I. C. R., Demarsy, E.,**
851 **Trevisan, M., Davis, P. A., Roelfsema, M. R. G., Hangarter, R.,**
852 **Fankhauser, C., et al.** (2013). D6PK AGCVIII kinases are required for

auxin transport and phototropic hypocotyl bending in Arabidopsis. *The Plant Cell* **25**, 1674–1688.

Wisniewska, J., Xu, J., Seifertová, D., Brewer, P. B., Ruzicka, K., Blilou, I., Rouquié, D., Benková, E., Scheres, B. and Friml, J. (2006). Polar PIN localization directs auxin flow in plants. *Science* **312**, 883–883.

Xu, J., Hofhuis, H., Heidstra, R., Sauer, M., Friml, J. and Scheres, B. (2006). A molecular framework for plant regeneration. *Science* **311**, 385–388.

Zhou, C., Han, L., Hou, C., Metelli, A., Qi, L., Tadege, M., Mysore, K. S. and Wang, Z.-Y. (2011). Developmental analysis of a Medicago truncatula smooth leaf margin1 mutant reveals context-dependent effects on compound leaf development. *The Plant Cell* **23**, 2106–2124.

Zourelidou, M., Absmanner, B., Weller, B., Barbosa, I. C. R., Willige, B. C., Fastner, A., Streit, V., Port, S. A., Colcombet, J., la Fuente van Bentem, de, S., et al. (2014). Auxin efflux by PIN-FORMED proteins is activated by two different protein kinases, D6 PROTEIN KINASE and PINOID. *eLife* **3**.

Figures and Legends

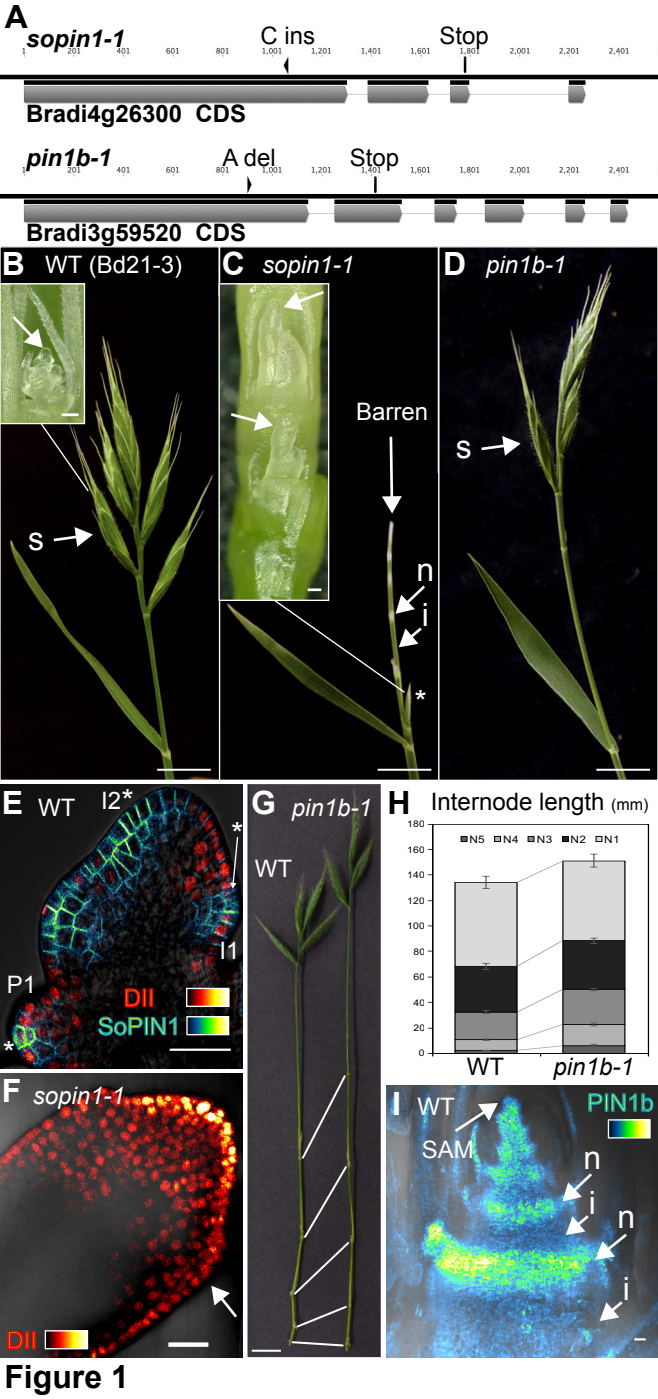
A
sopin1-1
C ins
Stop
Bradi4g26300 CDS
pin1b-1
A del
Stop
Bradi3g59520 CDS
B WT (Bd21-3)
s
C sopin1-1
Barren
n
i
*
D pin1b-1
s
E WT
I2*
I1
P1
DII
SoPIN1
F sopin1-1
DII
G pin1b-1
WT
H Internode length (mm)
N5 N4 N3 N2 N1
WT
pin1b-1
I WT
SAM
PIN1b
n
i
n
i

Figure 1

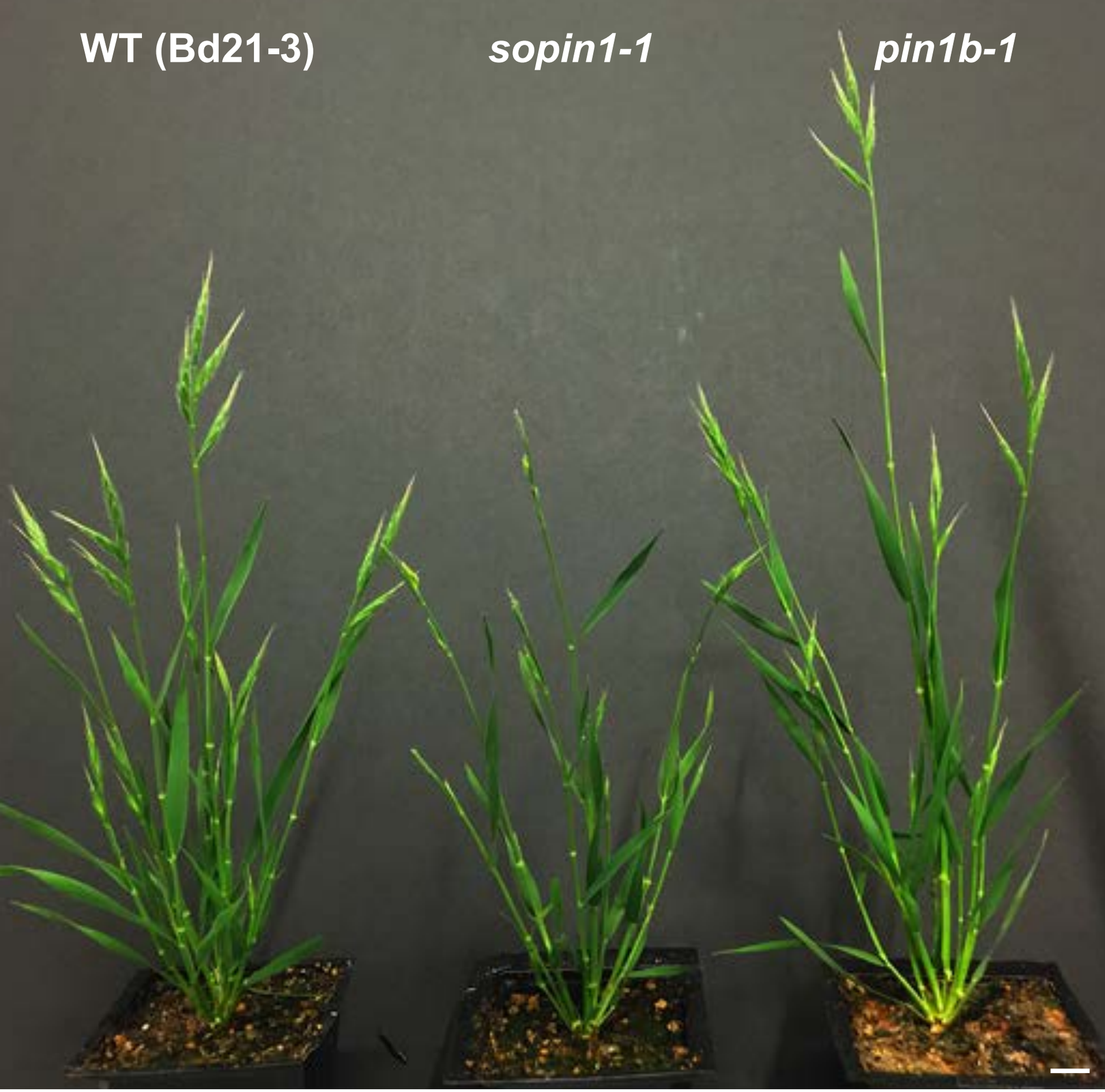

Figure 1 - supplement 1

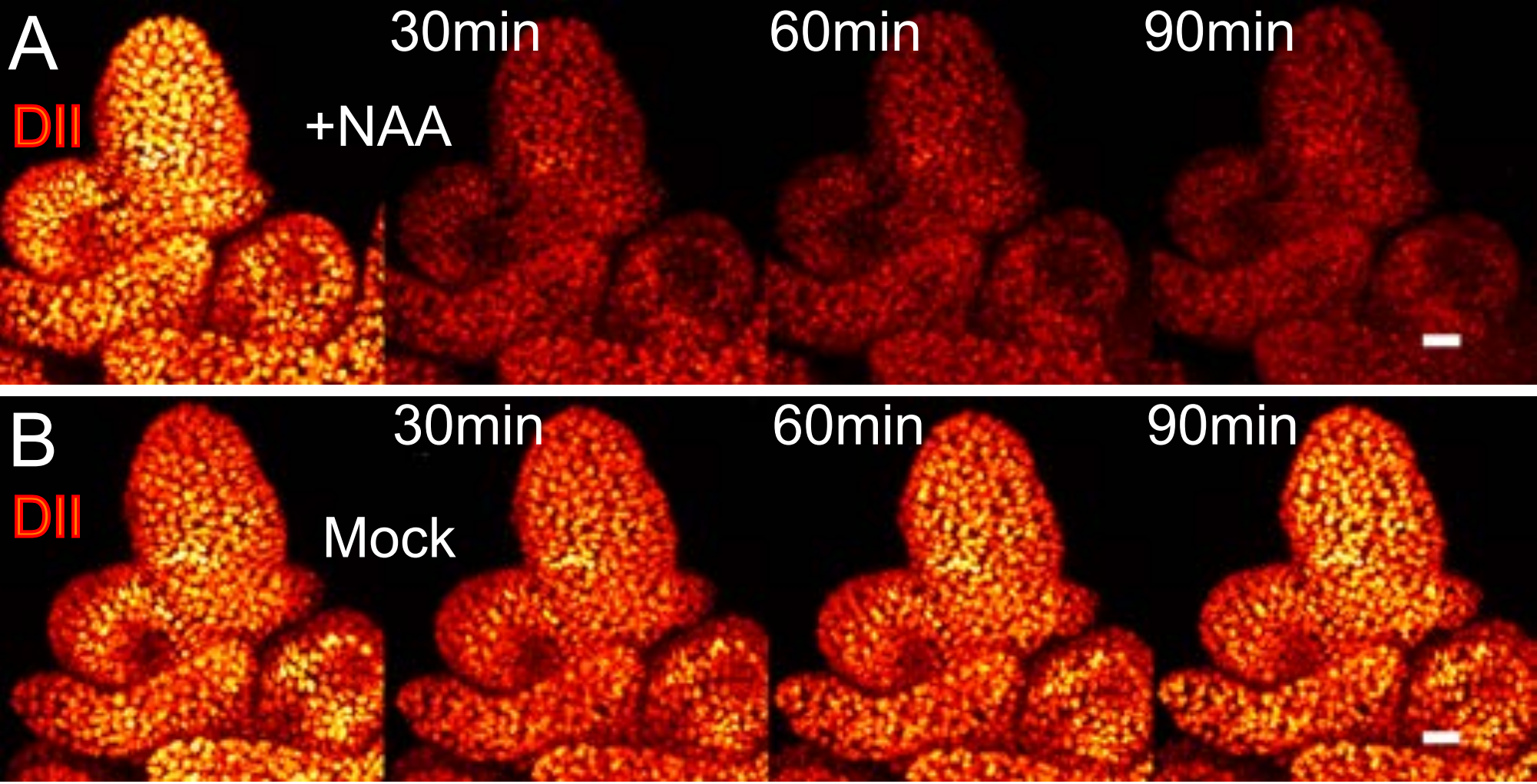

Figure 1 - supplement 2

875 **Figure 1. SoPIN1 and PIN1b have different functions in Brachypodium. (A)**
876 SoPIN1 (Bradi4g26300) and PIN1b (Bradi3g59520) CRISPR-derived *sopin1-1* and
877 *pin1b-1* mutant alleles. Exons are indicated by grey boxes. Arrowheads indicate
878 CRISPR target sites and are labeled with the type of DNA lesion (C insertion or A
879 deletion). Both alleles have premature stop codons at the positions indicated by lines.
880 **(B-D)** Inflorescence phenotypes of CRISPR-derived *sopin1-1* and *pin1b-1* mutants.
881 See Figure 1 – supplement 1 for whole-plant phenotypes. **(B)** Wildtype (WT) (inbred
882 line Bd21-3) Brachypodium inflorescences usually have several spikelets (s) on each
883 inflorescence. Inset shows spikelet meristem (arrow), with several floral meristems
884 being initiated. **(C)** *sopin1-1* plants have severe organ initiation defects in the
885 inflorescence, and spikelets often abort (asterisk), or fail to initiate despite a clear
886 distinction between the white node (n) and green internode (i) tissue. Inset shows two
887 barren spikelet meristems (arrows) with organ initiation defects. **(D)** *pin1b-1* plants
888 have normal organ initiation, but internode tissue often bends. A phenotypically normal
889 spikelet (s) is indicated. **(E)** Medial confocal Z-section of pZmUbi::DII-Venus (DII)
890 expression in a WT spikelet co-expressing SoPIN1 tagged with Cerulean (a CFP
891 variant) under the native SoPIN1 promoter. Organ primordia are numbered I2, I1 from
892 youngest to oldest prior to morphogenesis, and P1, P2, P3, etc. youngest to oldest
893 after morphogenesis. DII is normally degraded at SoPIN1 convergence points in I2
894 and I1 primordia (asterisks), and in response to auxin treatment (See Figure 1 –
895 supplement 2). Inset shows color look-up-table for all PIN images. **(F)** Medial confocal
896 Z-section of pZmUbi::DII-Venus expression in a *sopin1-1* spikelet meristem. DII
897 degradation does not occur in *sopin1-1* meristems, and organs fail to initiate (arrow).
898 Inset shows color look-up-table for DII. **(G-H)** Basal internodes are elongated in *pin1b-*
899 *1* mutants compared to WT. Lines in **(G)** connect equivalent nodes in WT (left) and

pin1b-1 (right) primary stems. Axillary shoots and leaves have been removed from the main axis. **(H)** Mean internode lengths along WT (left) and *pin1b-1* (right) primary stems. Nodes are numbered from 1 starting from below the inflorescence. (n=11-12 each internode, error bars +/- standard error of the mean). See Figure 1 - Source Data 1 for source data. **(I)** Maximum projection of PIN1b tagged with Citrine under its native promoter in a longitudinal hand-section through several immature vegetative nodes**.** Arrows indicate the shoot apical meristem (SAM), node (n), and internode (i) tissues. Scale bars: 1cm in **(B-D)** and **(G)**. 25µm in **(E)**, **(F)** and **(I)**.

Figure 1 – supplement 1. Mature whole-plant phenotypes of Brachypodium CRISPR-derived *sopin1-1* and *pin1b-1* mutants. Left WT (Inbred Bd21-3), middle *sopin1-1,* and right *pin1b-1.* Scale bar: 1cm.

Figure 1 – supplement 2. DII-Venus is degraded in the presence of auxin in Brachypodium spikelet meristems. (A) 1 µM NAA-treated, and **(B)** mock-treated spikelet meristems expressing pZmUbi::DII-Venus imaged every 30 min after treatment. Images from left to right, pre-treatment expression, 30 min, 60 min and 90 min time-points. Scale bars: 25µm.

Figure 1 - Source Data 1. Source data for internode length measurements displayed in Figure 1H.

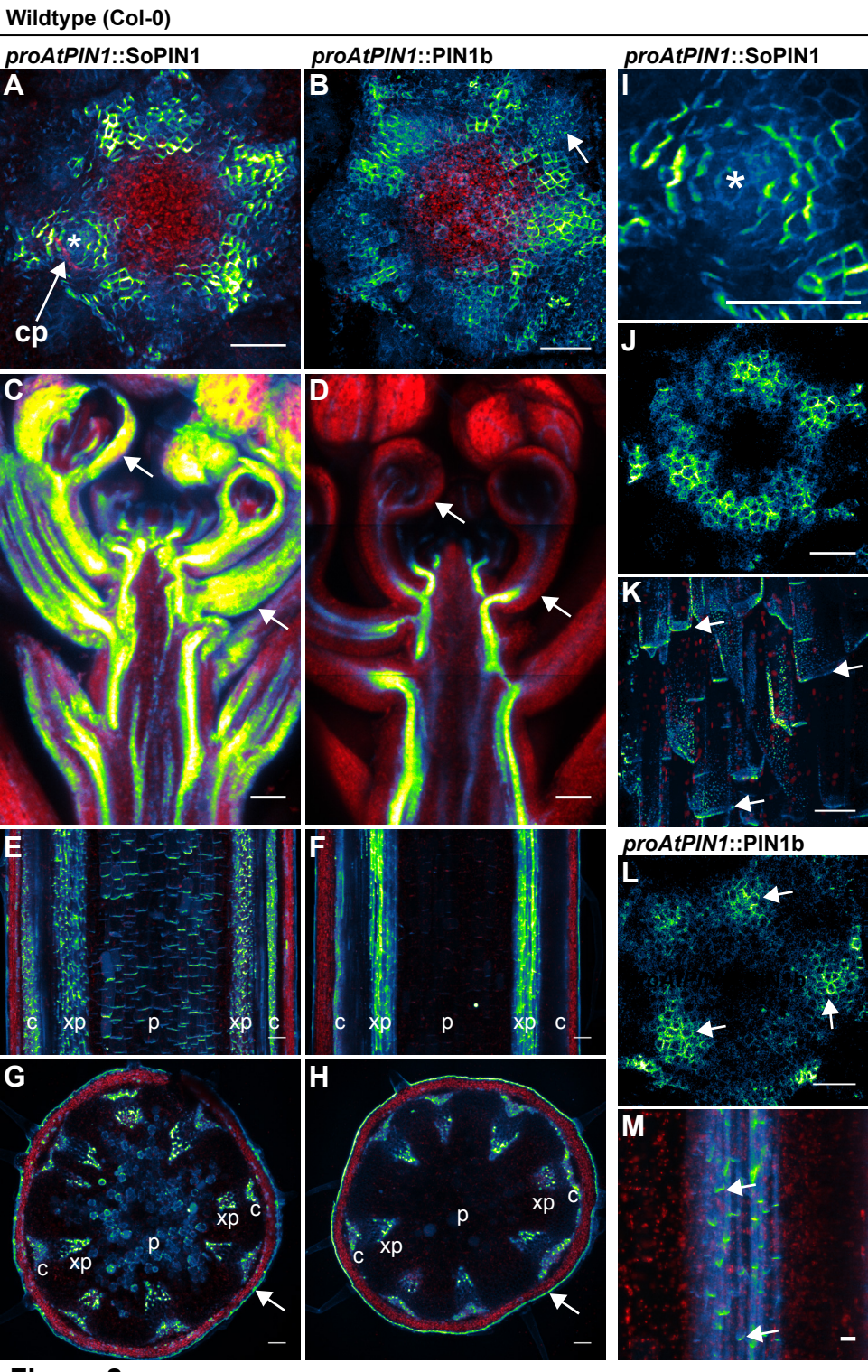
Wildtype (Col-0)
proAtPIN1::SoPIN1
proAtPIN1::PIN1b
proAtPIN1::SoPIN1
A
B
I
*
cp
C
D
J
K
E
F
proAtPIN1::PIN1b
L
c
xp
p
xp
c
G
H
M

Figure 2

Figure 2. SoPIN1 and PIN1b show different behaviors when expressed in wildtype Arabidopsis. Arabidopsis *AtPIN1* promoter (*proAtPIN1*) driven expression of Citrine-tagged (a YFP derivative) SoPIN1 and PIN1b in wildtype Columbia (Col-0) Arabidopsis. **(A,C,E,G,I,J,K)** SoPIN1, **(B,D,F,H,L,M)** PIN1b. **(A-B)** Maximum projections of meristem apexes. Arrow in **(A)** indicates SoPIN1 convergence point (cp) in an I2 primordium. Arrow in **(B)** indicates internalized PIN1b in punctate membrane bodies. **(C-D)** Tiled confocal maximum projections of longitudinal hand-sections through apexes. Arrows indicate SoPIN1 epidermal expression in sepal primordia and flower pedicels in **(C)** and the lack of PIN1b epidermal expression in the same tissues in **(D)**. **(E-F)** Tiled confocal maximum projections of longitudinal sections through basal inflorescence stem internodes 1cm above the rosette. **(G-H)** Tiled confocal maximum projections of cross-sections through basal internodes 1cm above the rosette. Signal at the edge of each section (arrows) is cuticle auto-florescence. The cambium (c), xylem parenchyma (xp), and pith (p) tissues are indicated in **(E-H). (I)** Maximum projection detail of SoPIN1 convergence point (Asterisk) in I2 primordia in meristem shown in **(A)**. **(J)** Confocal z-section of SoPIN1 accumulation in a ring-shaped domain just below the apex of the meristem shown in **(A)**. **(K)** Maximum projection detail of root-ward polarized SoPIN1 (arrows) in a longitudinal section of the basal internode pith tissue. **(L)** Confocal z-section of PIN1b accumulation in distinct vascular-associated domains just below the apex of the meristem shown in **(B)**. **(M)** Maximum projection detail of root-ward polarized PIN1b (arrows) in a longitudinal section of the basal internode xylem parenchyma tissue. Red signal in all panels is chlorophyll auto-florescence. Scale bars: 25μm in **(A-B),** 100μm in **(C-H),** and 25μm in **(I-M)**.

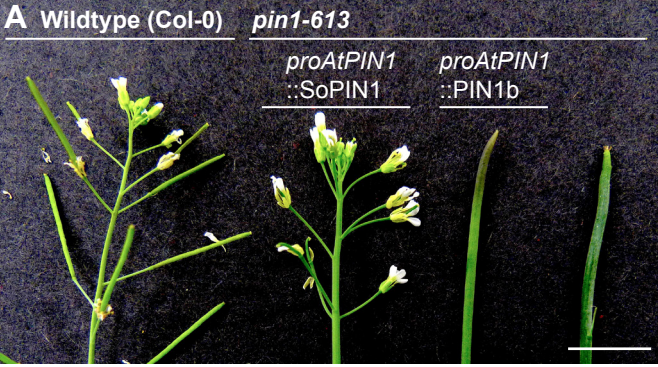
A Wildtype (Col-0)
pin1-613
proAtPIN1 ::SoPIN1
proAtPIN1 ::PIN1b

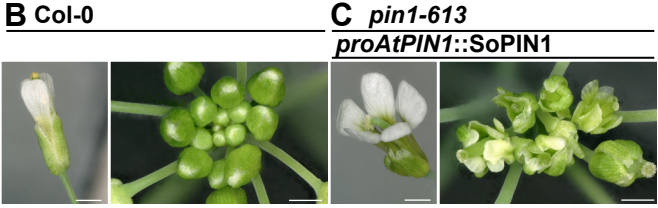
B Col-0
C pin1-613
proAtPIN1::SoPIN1

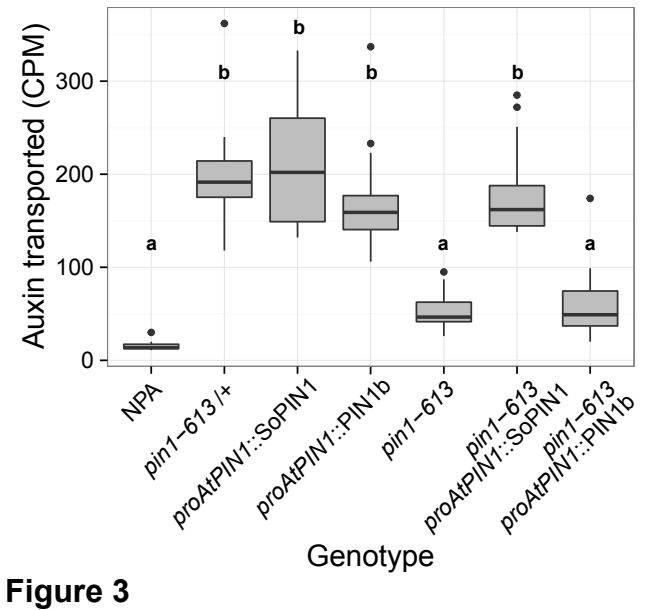
D Stem auxin transport
Auxin transported (CPM)
0
100
200
300
a
b
b
b
a
b
a
NPA
pin1−613/+
proAtPIN1::SoPIN1
proAtPIN1::PIN1b
pin1−613
pin1−613 proAtPIN1::SoPIN1
pin1−613 proAtPIN1::PIN1b
Genotype

Figure 3

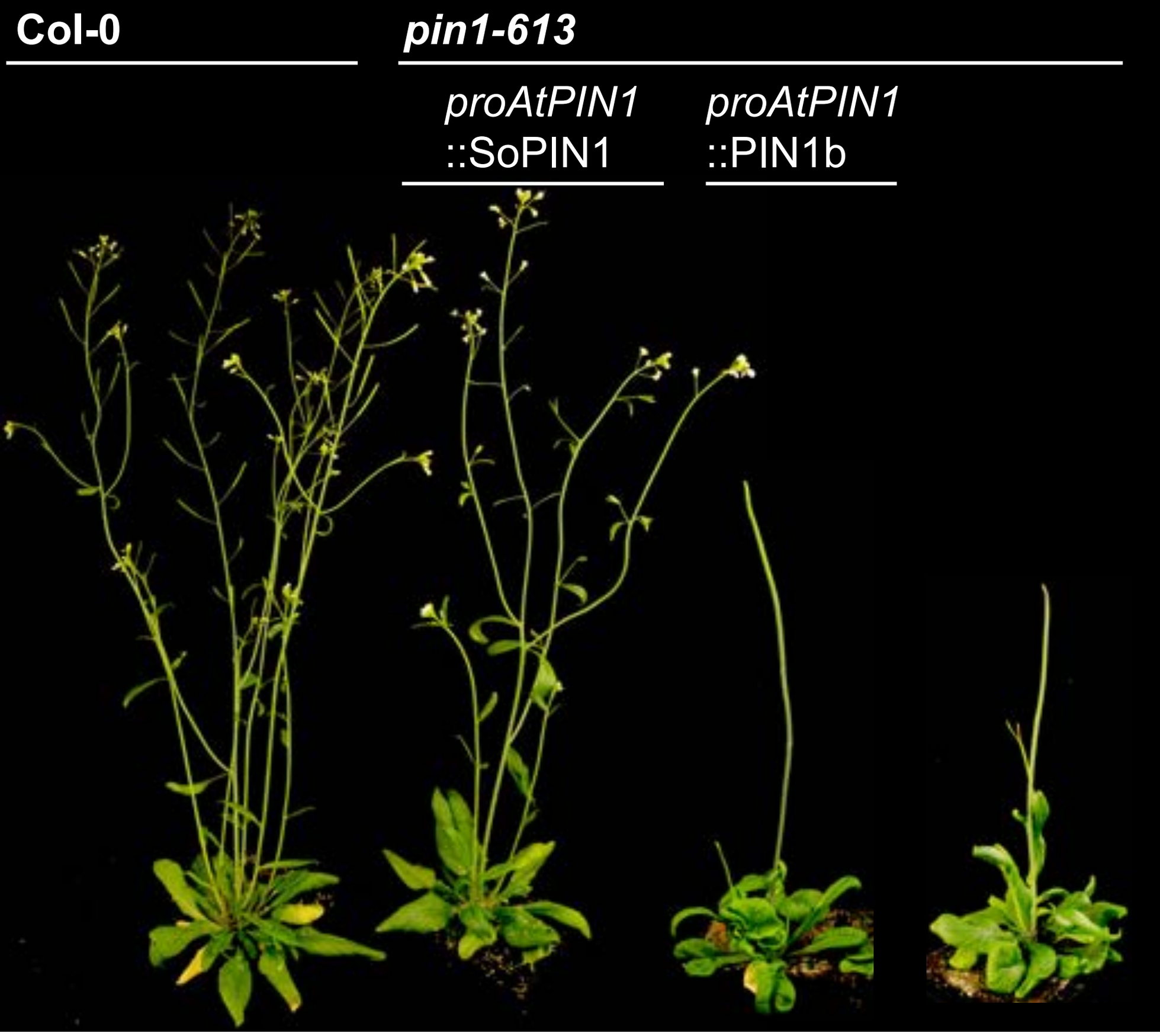

Figure 3 - supplement 1

Floral organ number - *proAtPIN1::*SoPIN1

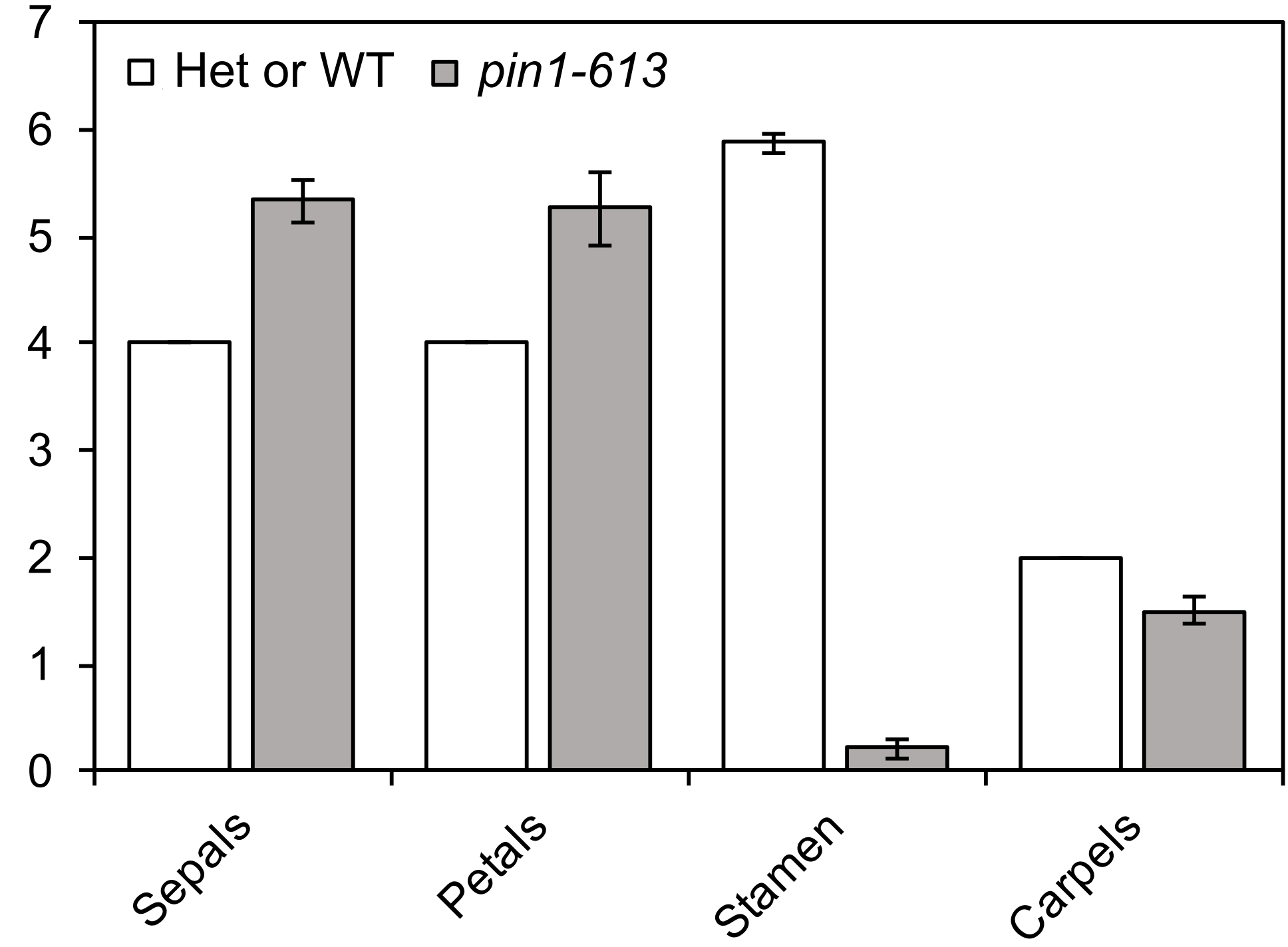

Figure 3 - supplement 2

946 **Figure 3. SoPIN1 but not PIN1b can partially complement the Arabidopsis *pin1-***
947 ***613* mutant organ initiation and bulk transport defects. (A)** From left to right,
948 inflorescence phenotypes of WT (Col-0), *proAtPIN1::*SoPIN1 in *pin1-613,*
949 *proAtPIN1*::PIN1b in *pin1-613,* and *pin1-613* alone. Note that PIN1b-expressing *pin1-*
950 *613* plants are indistinguishable from *pin1-613* alone. See Figure 3 - supplement 1 for
951 whole-plant phenotypes. **(B)** Flower (left), and inflorescence apex (right) of WT (Col-
952 0). **(C)** Flower (left), and inflorescence apex (right) of *proAtPIN1::*SoPIN1
953 complemented *pin1-613* mutants. Note the increase in petal number and lack of
954 stamens in the flower, see Figure 3 - supplement 2 for organ counts. **(D)** Box-plot of
955 bulk auxin transport (counts per minute, CPM) through basal internodes 1cm above
956 the rosette of 40-day-old Arabidopsis inflorescence stems. (n=16 each genotype).
957 Samples with different letters are significantly different from each other (ANOVA,
958 Tukey HSD, $p < 0.05$). See Figure 3 - Source Data 1 for source data. Scale bars: 1cm
959 in **(A)**, 1mm in **(B-C)**.
960
961 **Figure 3 - supplement 1. Whole-plant phenotypes of *proAtPIN1*-driven**
962 **complementation of *pin1-613.*** From left to right, Col-0 (WT), *proAtPIN1::*SoPIN1
963 complemented *pin1-613*, *proAtPIN1::*PIN1b expressing *pin1-613, pin1-613.*
964
965 **Figure 3 - supplement 2. Floral organ number in *proAtPIN1::*SoPIN1**
966 **complemented flowers.** Mean and standard-error of sepal, petal, stamen and carpel
967 organ numbers in heterozygous *pin1-613* or wildtype (white bars), and
968 *proAtPIN1::*SoPIN1-complemented *pin1-613* flowers (grey bars) (n=30). See Figure 3
969 - Source Data 2 for source data.
970

971 **Figure 3 - Source Data 1. Source data for Figure 3D auxin transport assays.**

972 **Figure 3 - Source Data 2. Source data for Figure 3 - supplement 2 floral organ**

973 **numbers.**

974

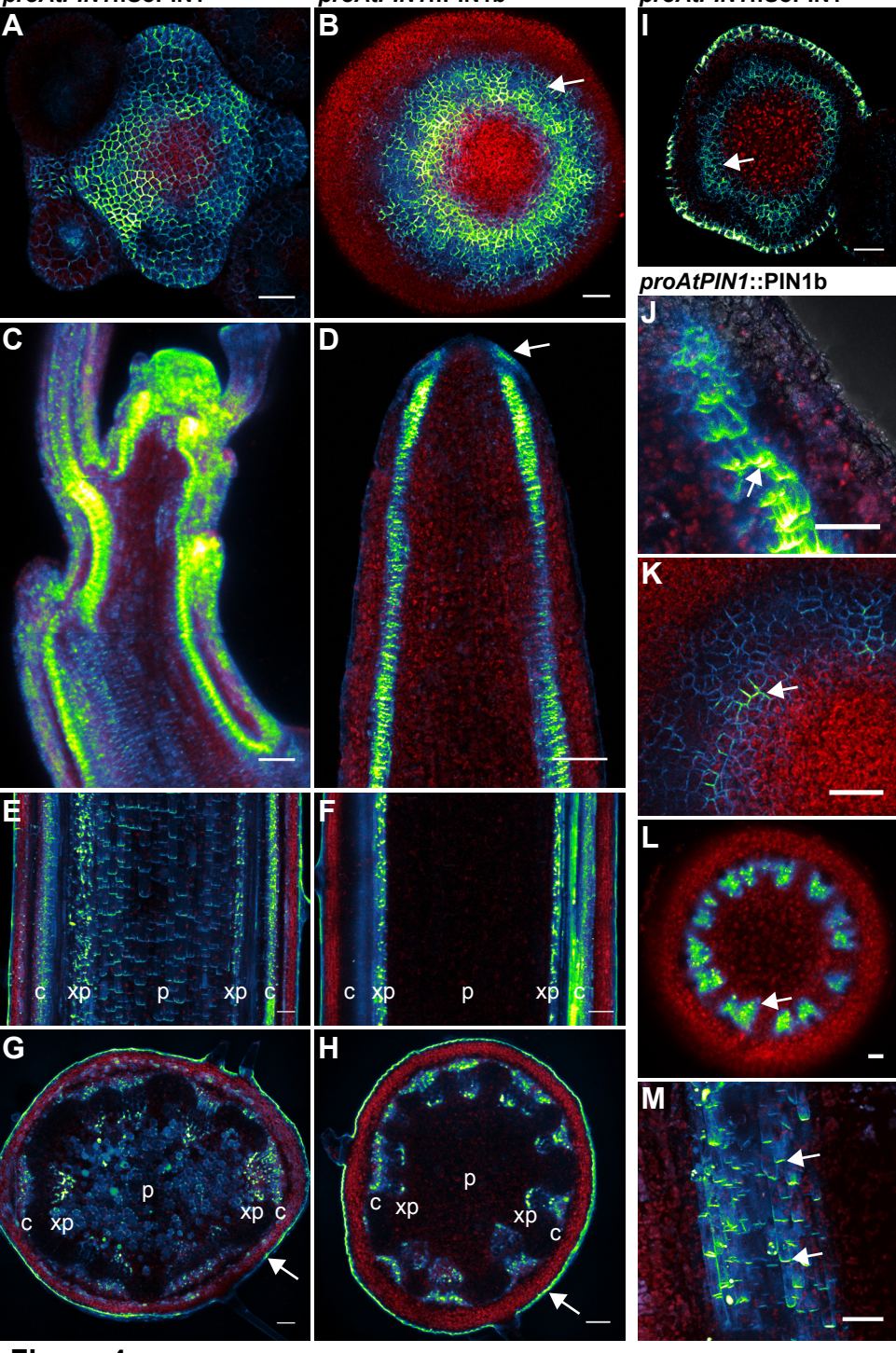
proAtPIN1::SoPIN1
proAtPIN1::PIN1b
proAtPIN1::SoPIN1
proAtPIN1::PIN1b
A
B
I
C
D
J
K
E
F
L
G
H
M
c
xp
p
xp
c

Figure 4

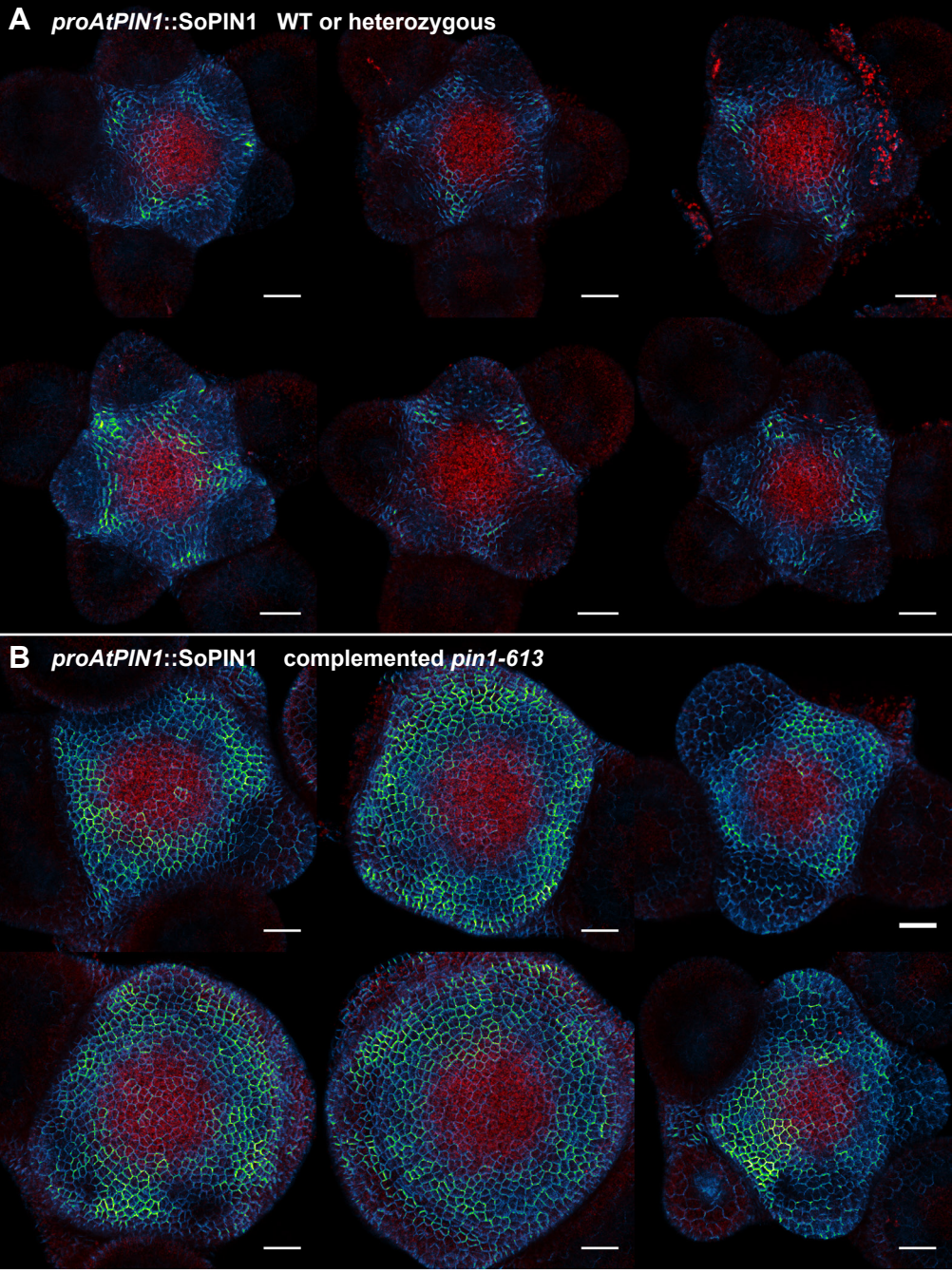

Figure 4 - supplement 1

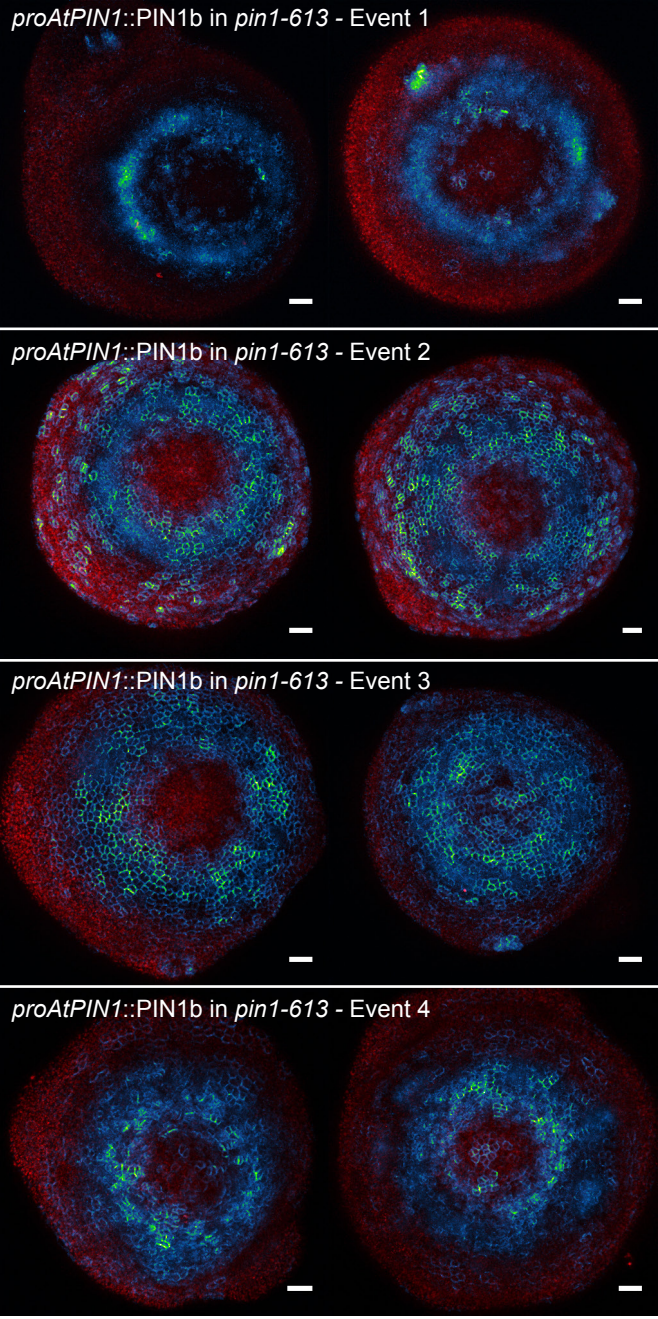

Figure 4 - supplement 2

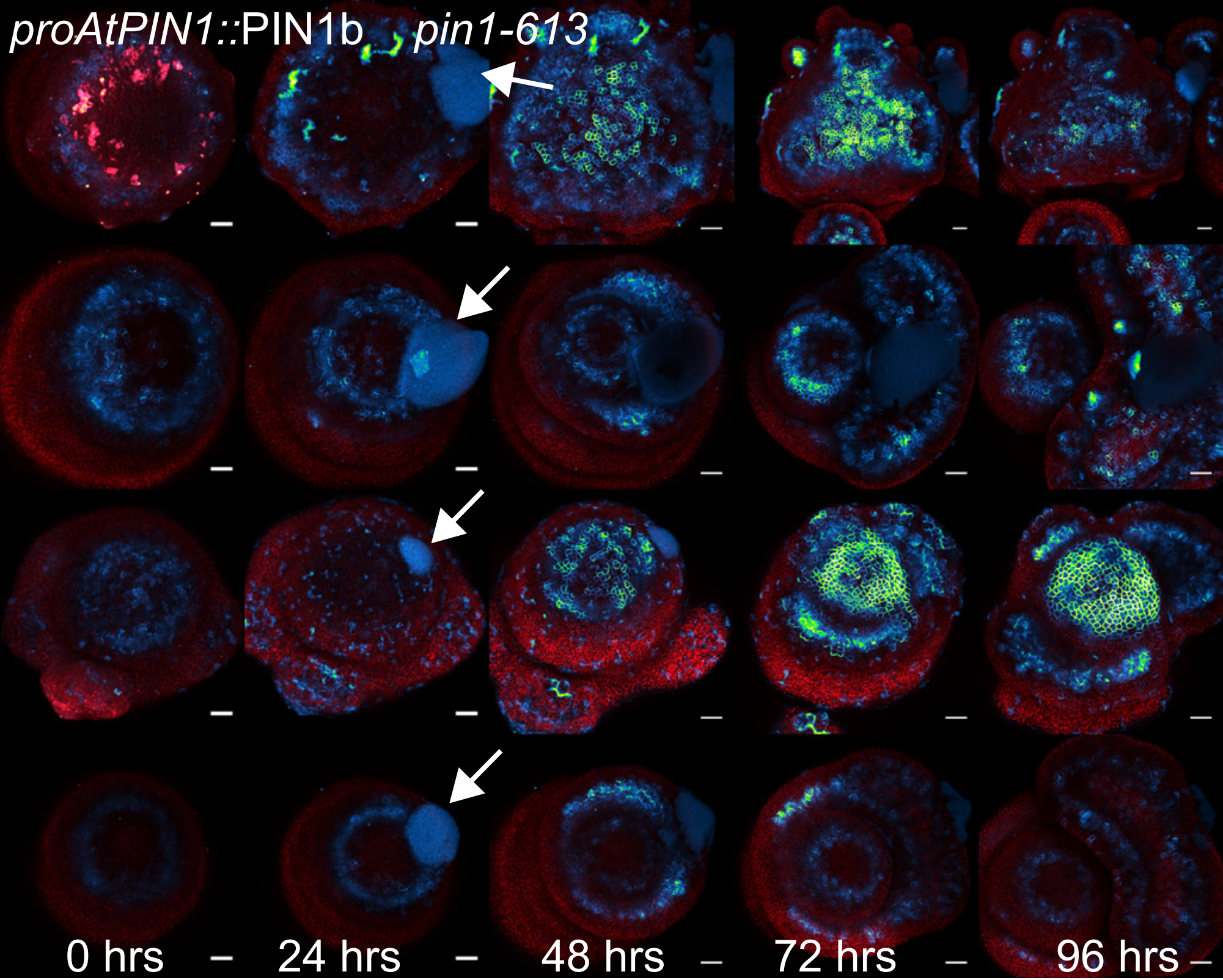

Figure 4 - supplement 3

975 **Figure 4. SoPIN1 but not PIN1b can mediate organ initiation and bulk transport**
976 **in null *pin1-613 mutants*.** Arabidopsis *PIN1* promoter (*proAtPIN1*) driven expression
977 of Citrine-tagged (YFP derivative) SoPIN1 and PIN1b in null *pin1-613* mutant tissue.
978 **(A,C,E,G,I)** SoPIN1, **(B,D,F,H,J,K,L,M)** PIN1b. **(A-B)** Maximum projections of
979 meristem apexes. Arrow in **(B)** indicates PIN1b ring shaped epidermal domain. See
980 Figure 4 – supplement 1 for SoPIN1 expression in a *pin1-613* segregating family. See
981 Figure 4 – supplement 2 for more examples of PIN1b expression in *pin1-613* apexes,
982 and Figure 4 – supplement 3 for PIN1b dynamics in response to auxin addition. **(C-D)**
983 Tiled confocal maximum projections of longitudinal hand-sections through apexes.
984 Arrow in **(D)** indicates increased PIN1b in the epidermis in the *pin1-613* background.
985 **(E-F)** Tiled maximum projections of longitudinal sections through basal inflorescence
986 stem internodes 1cm above the rosette. **(G-H)** Tiled maximum projections of cross-
987 sections through basal internodes 1cm above the rosette. Signal at the edge of each
988 section (arrows) is cuticle auto-florescence. The cambium (c), xylem parenchyma (xp),
989 and pith (p) tissues are indicated in **(E-H). (I)** Confocal z-section of SoPIN1
990 accumulation in a ring-shaped domain just below the apex of a complemented *pin1-*
991 *613* meristem. **(J)** Longitudinal hand-section of PIN1b just below a *pin1-613* meristem
992 apex. Arrow shows root-ward polarized PIN1b. **(K)** Detail of polarized PIN1b in the
993 meristem epidermis of a *pin1-613* meristem apex. **(L)** Cross-section of PIN1b in
994 distinct bundles 2mm below a *pin1-613* meristem apex. **(M)** Root-ward polarization of
995 PIN1b (arrow) 3-4 mm below the apex of a *pin1-613* meristem. Red signal in all panels
996 is chlorophyll auto-florescence. Scale bars: 25μm in **(A-B),** 100μm in **(C-H),** and 25μm
997 in **(I-M)**.
998

Figure 4 – supplement 1. *proAtPIN1::*SoPIN1 expression in *pin1-613* segregating family. (A) *proAtPIN1::*SoPIN1 expression in 6 different WT or heterozygous *pin1-613* meristem samples. **(B)** *proAtPIN1::*SoPIN1 expression in 6 different complemented *pin1-613* meristems. All samples were imaged with identical settings to show the increase in SoPIN1 in the *pin1-613* mutant background. Red signal is chlorophyll auto-florescence. Scale bars: 25µm.

Figure 4 – supplement 2. *proAtPIN1::*PIN1b expression in *pin1-613* apexes. Two representative meristems each from four different transgenic events. All samples were imaged with identical settings. Scale bars: 25µm.

Figure 4 – supplement 3. *proAtPIN1::*PIN1b dynamics during organ formation induced by addition of lanolin containing 1mM IAA on *pin1-613* apexes. From left to right, pre-treatment, 24, 48, 72, and 96 hours after treatment. Four representative samples are shown top to bottom. Arrows indicate the lanolin paste at the 24-hour time-point. All samples were imaged with identical settings. Scale bars 25µm.

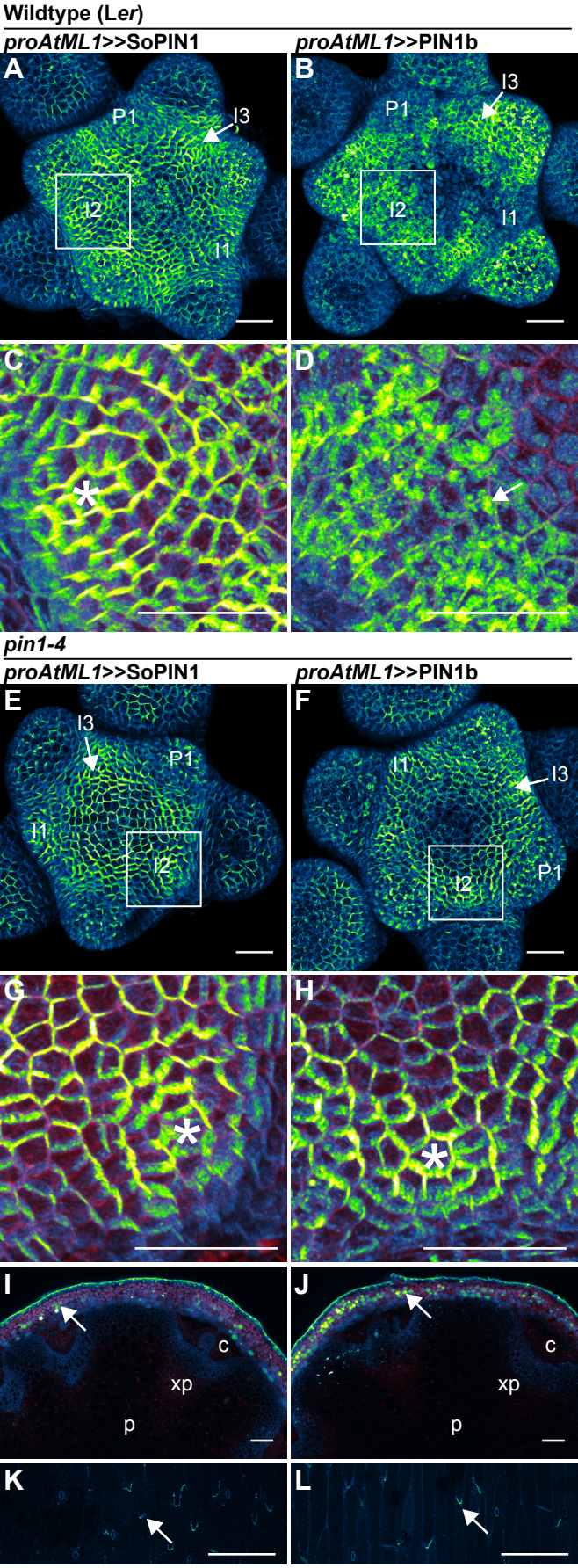
Wildtype (Ler)
proAtML1>>SoPIN1
proAtML1>>PIN1b
A
P1
I3
I2
I1
B
P1
I3
I2
I1
C
D
pin1-4
proAtML1>>SoPIN1
proAtML1>>PIN1b
E
I3
P1
I1
I2
F
I1
I3
I2
P1
G
H
I
c
xp
p
J
c
xp
p
K
L

Figure 5

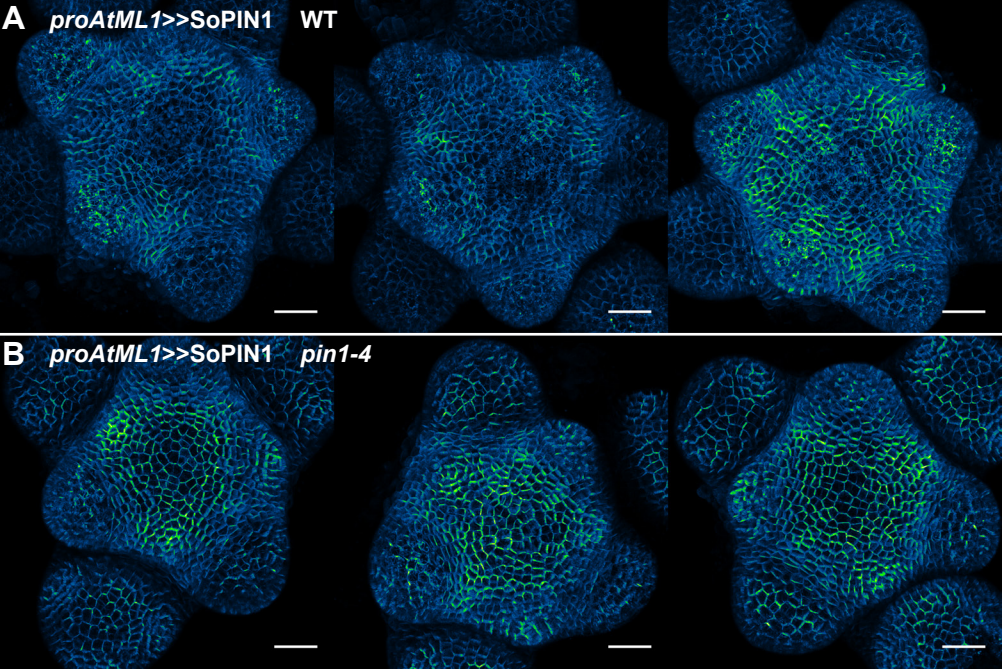

Figure 5 - supplement 1 - *proAtML1*>>SoPIN1

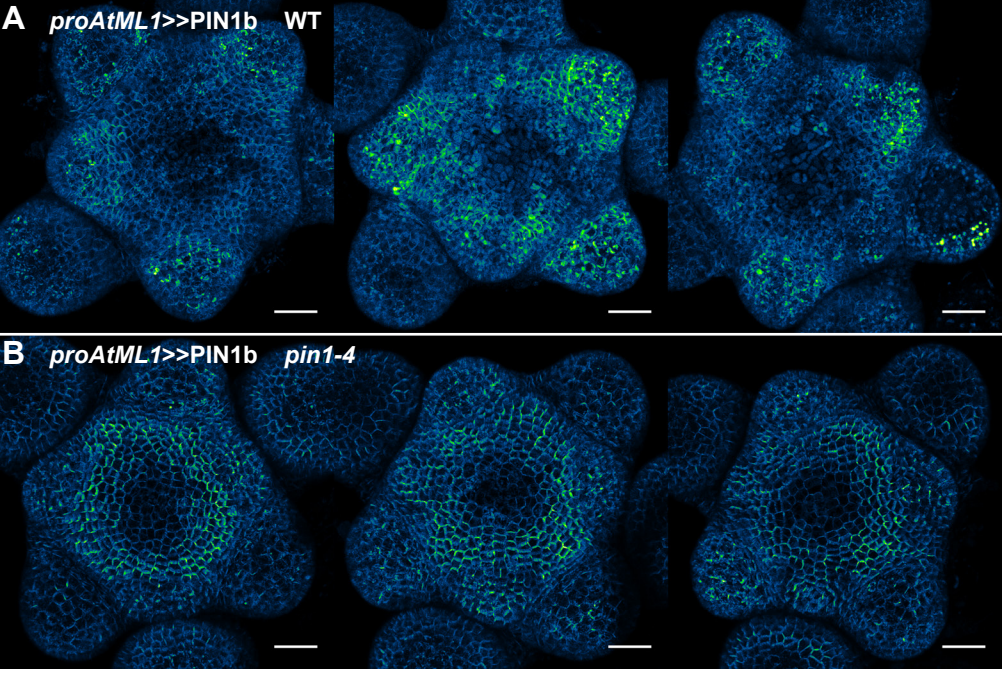

Figure 5 - supplement 2 - *proAtML1*>>PIN1b

Figure 5. SoPIN1 and PIN1b show different behaviors under *proAtML1*-driven expression. Maximum projections of *proAtML1::*LhG4 driving pOP::SoPIN1 or pOP::PIN1b (*proAtML1*>>SoPIN1 and *proAtML1*>>PIN1b) in wildtype Landsberg *erecta* (L*er)* **(A-D),** and *pin1-4* **(E-L)** inflorescence meristems and basal internodes. **(A)** SoPIN1 and **(B)** PIN1b maximum projections of wildtype L*er* inflorescence meristems. I3, I2, I1, and P1 primordia are indicated. White boxes around each I2 primordium indicate the regions detailed in **(C-D).** Asterisk in **(C)** indicates convergence point. Arrow in **(D)** indicates punctate PIN1b. **(E)** SoPIN1 and **(F)** PIN1b maximum projections of complemented *pin1-4* meristems. I3, I2, I1, and P1 primordia are indicated. White boxes around each I2 primordia indicate the regions detailed in **(G-H)**. Asterisks mark convergence points in **(G)** and **(H)**. Red signal in **(C,D,G,H)** is cell wall propidium iodide staining. See Figure 5 – supplement 1 for additional samples of *proAtML1*>>SoPIN1 and Figure 5 – supplement 2 for additional samples of *proAtML1*>>PIN1b in both WT and *pin1-4* meristems. **(I-J)** Tiled maximum projections of cross hand-sections of the basal internode of SoPIN1 **(I)** and PIN1b **(J)** - complemented *pin1-4* plants showing PIN signal in the outer cortex layers (arrows). Red signal in **(I-J)** is chlorophyll auto-florescence. **(K-L)** Epidermal maximum projections showing root-ward polarized PIN localization (arrows) in the basal internode of SoPIN1 **(K),** and PIN1b **(L) -**complemented *pin1-4* plants. Scale bars: 25µm in **(A-H)**. 100µm in **(I-L)**.

Figure 5 – supplement 1. *proAtML1*>>SoPIN1 representative meristem maximum projections. (A) *proAtML1*>>SoPIN1 expression in three different wildtype L*er* meristems. **(B)** *proAtML1*>>SoPIN1 expression in three different complemented *pin1-4* meristems. Capture settings are identical in all samples. Scale bars: 25µm.

Figure 5 – supplement 2. *proAtML1*>>PIN1b representative meristem maximum projections. (A) *proAtML1*>>PIN1b expression in three different wildtype L*er* meristems. **(B)** *proAtML1*>>PIN1b expression in three different complemented *pin1-4* meristems. Capture settings are identical in all samples. Scale bars: 25µm.

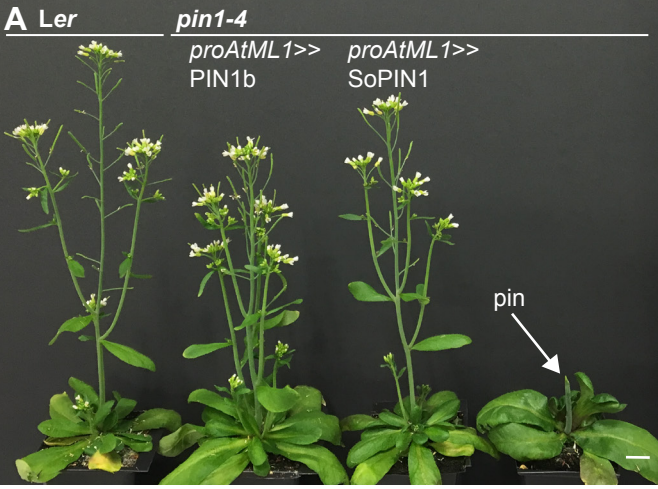
A Ler
pin1-4
proAtML1>>
PIN1b
proAtML1>>
SoPIN1
pin

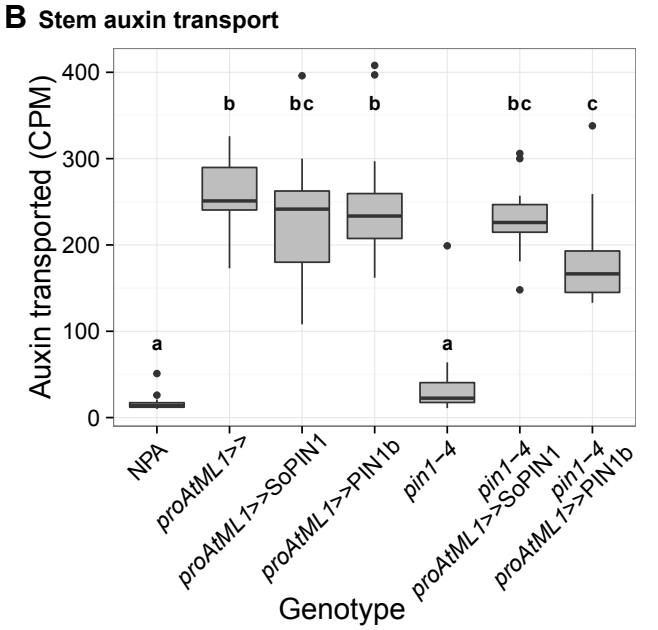
B Stem auxin transport
Auxin transported (CPM)
400
300
200
100
0
a
b
bc
b
a
bc
c
NPA
proAtML1>>
proAtML1>>SoPIN1
proAtML1>>PIN1b
pin1−4
pin1−4 proAtML1>>SoPIN1
pin1−4 proAtML1>>PIN1b
Genotype

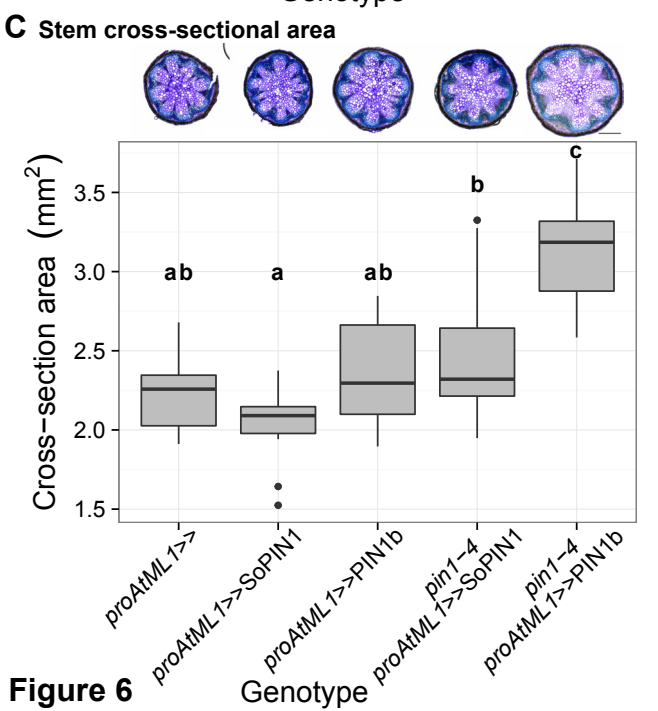
C Stem cross-sectional area
Cross−section area (mm2)
3.5
3.0
2.5
2.0
1.5
ab
a
ab
b
c
proAtML1>>
proAtML1>>SoPIN1
proAtML1>>PIN1b
pin1−4 proAtML1>>SoPIN1
pin1−4 proAtML1>>PIN1b
Genotype

Figure 6

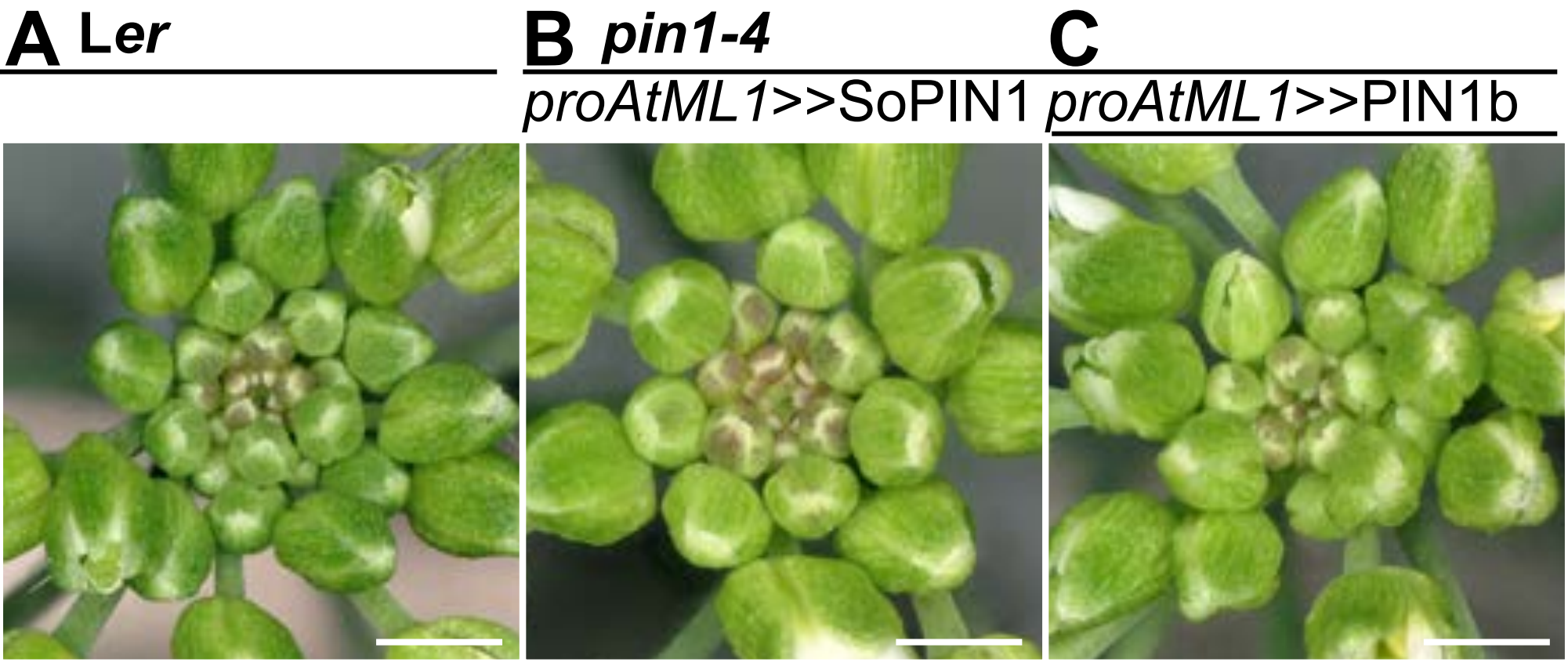

Figure 6 - supplement 1

Figure 6. Both SoPIN1 and PIN1b can complement *Arabidopsis pin1-4* under *proAtML1*-driven expression. (A) From left to right, wildtype *Ler, proAtML1*>>PIN1b complemented *pin1-4, proAtML1*>>SoPIN1 complemented *pin1-4, and pin1-4 alone.* Arrow indicates barren pin inflorescence in *pin1-4*. See Figure 6 – supplement 1 for inflorescence phenotypes. **(B)** Box-plot of bulk auxin transport (counts per minute, CPM) through basal internodes 1cm above the rosette of 40-day-old Arabidopsis inflorescence stems (n=16 each genotype). Samples with different letters are significantly different from each other (ANOVA, Tukey HSD, $p < 0.05$). See Figure 6 - Source Data 1 for source data. **(C)** Box-plot of stem cross-sectional area (square mm) of the basal internode 1cm above the rosette (n=12 each genotype). Representative Toluidine Blue O stained hand cross-sections are shown above each box. Samples with different letters are significantly different from each other. (ANOVA, Tukey HSD, $p < 0.05$). See Figure 6 - Source Data 2 for source data. *Scale* bars: 1cm in **(A)**. 500µm in **(C).**

Figure 6 – supplement 1. *proAtML1*>>SoPIN1 and *proAtML1*>>PIN1b complemented *pin1-4* inflorescence phenotypes. (A) Wildtype Ler, **(B)** *proAtML1*>>SoPIN1 complemented *pin1-4,* and **(C)** *proAtML1*>>PIN1b complemented *pin1-4* inflorescence apexes. Scale bars: 1mm.

Figure 6 - Source Data 1. Source data for Figure 6B auxin transport assays.

Figure 6 - Source Data 2. Source data for Figure 6C stem cross-sectional area measurements.

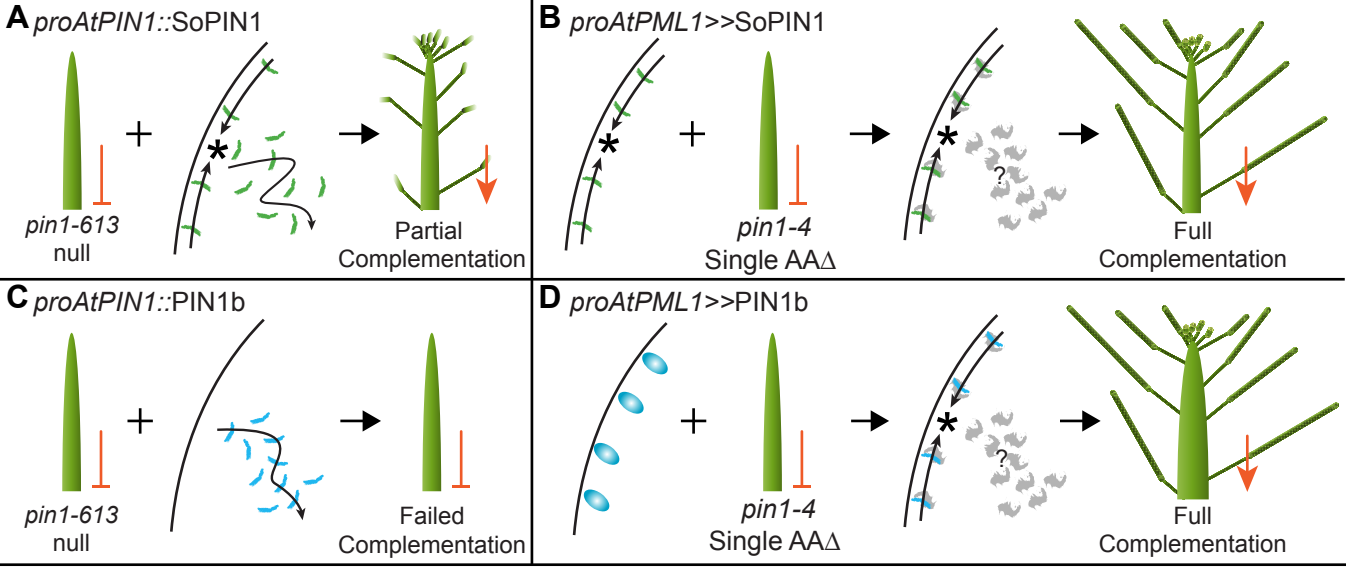
A proAtPIN1::SoPIN1
pin1-613
null
Partial
Complementation
B proAtPML1>>SoPIN1
pin1-4
Single AAΔ
Full
Complementation
C proAtPIN1::PIN1b
pin1-613
null
Failed
Complementation
D proAtPML1>>PIN1b
pin1-4
Single AAΔ
Full
Complementation
SoPIN1
PIN1b
Non-polarized PIN1b
pin1-4
Polarity
Convergence Point
Transport

Figure 7

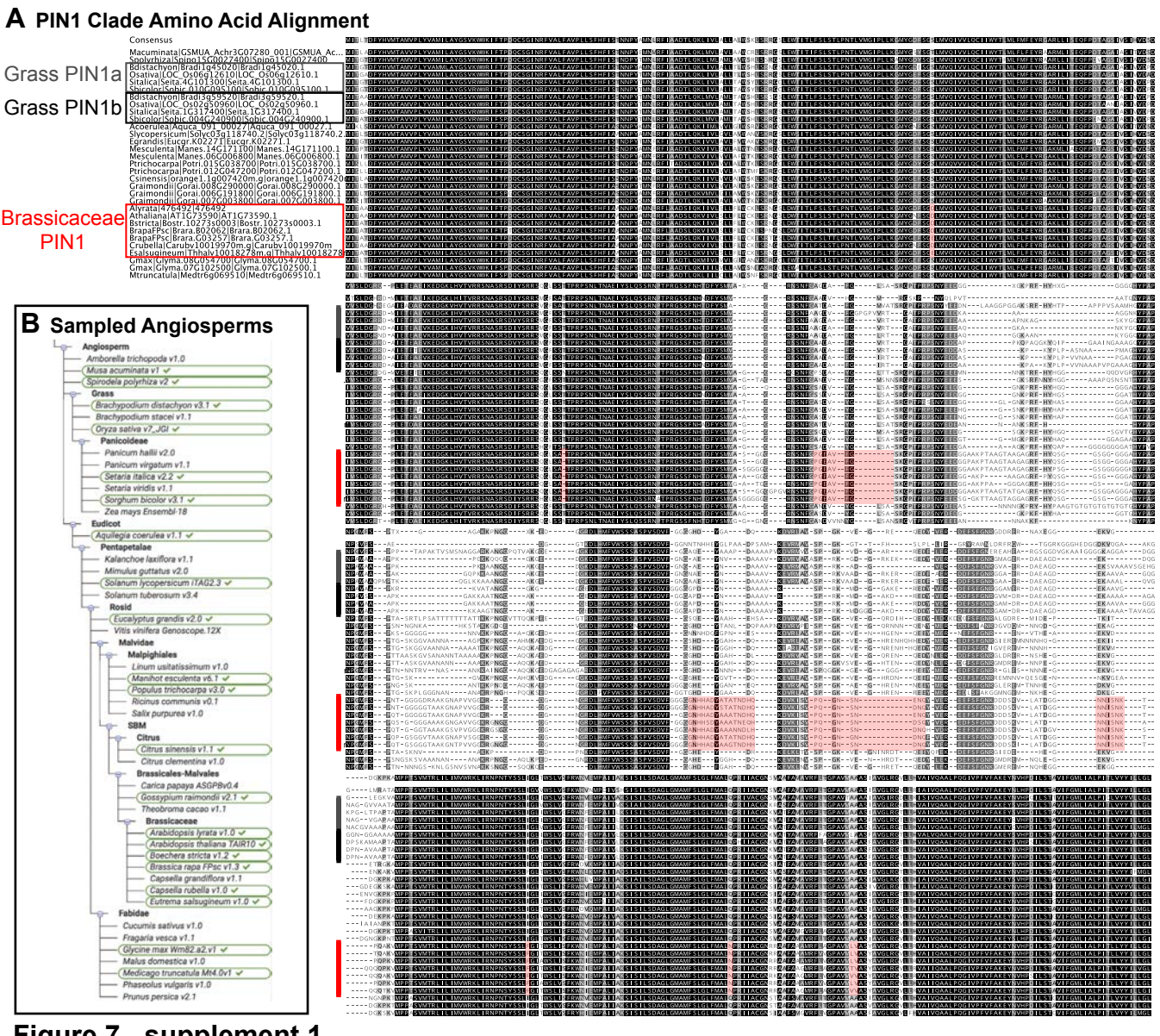

Figure 7 - supplement 1

Table 1: Primers

ID#	Name	Sequence	Purpose
1	019 - Ubi-1 Prom attB4 F	GGGGACAACTTTGTATAGAAAAGTTGCTGCAGTGCAGCGTGACCCGG	pZmUbi amplification for cloning
2	020 - Ubi-1 Prom attB1 R	GGGGACTGCTTTTTTGTACAAACTTGCTGCAGAAGTAACACCAAACA	pZmUbi amplification for cloning
3	PIN1pro-GW-F	GGGGACAACTTTGTATAGAAAAGTTGTTACCCTCATCCATCATTAACTT	*proAtPIN1* amplification
4	PIN1pro-GW-R	GGGGACTGCTTTTTTGTACAAACTTGTCTTTTGTTCGCCGGAGAAGAGA	*proAtPIN1* amplification
5	455 BdSoPIN1 cacc mRNA	TCACATCTGCTGCCGCTGCC	SoPIN1-Citrine coding region amplification
6	302 - PIN_7 qPCR UTR R2	AATCCCAAAAGCCGACATTG	SoPIN1-Citrine coding region amplification
7	466 BdPIN1b cacc mRNA-2	CACCTGTACACACTGCGGCGCT	PIN1b-Citrine coding region amplification
8	308 - PIN_5 qPCR UTR R1	ACTCGCTAACCAACCCCTTAATT	PIN1b-Citrine coding region amplification
9	MVR087 - pin1-613 RP (SALK_047613)	AATCATCACAGCCACTGATCC	*pin1-613* genotyping
10	MVR086 - pin1-613 LP (SALK_047613)	CAAAAACACCCCCAAAATTTC	*pin1-613* genotyping
11	MVR036 - LBb1.3	ATTTTGCCGATTTCGGAAC	*pin1-613* genotyping
12	344 - Citrine Seq R	GAAGCACATCAGGCCGTAG	PIN1b-Citrine and SoPIN1-Citrine genotyping
13	524_Bradi4g26300_4230_F	CGTTCCGTGTTGATTCCGATG	SoPIN1-Citrine genotyping
14	541_Bradi3g59520_PIN1b_5084_F	TGATGCTCTTCATGTTCGAGTACC	PIN1b-Citrine genotyping
15	543_pin1-4_Aci_F	GCTTTTGCGGCGGCTATGAGATTTGT	*pin1-4* genotyping
16	544_pin1-4_Aci_R	GCTTCTGATTTAATTTGTGGGTTTTCA	*pin1-4* genotyping
17	076 - BASTA_F2	CTTCAGCAGGTGGGTGTAGAG	ML1::LhG4 genotyping
18	077 - BASTA_R2	GAGACAAGCACGGTCAACTTC	ML1::LhG4 genotyping

Figure 7. Heterologous expression summary: Functional distinction between PIN auxin efflux proteins during development. Polarized SoPIN1 is represented by green lines, polarized PIN1b by blue lines, un-polarized PIN1b by blue circles, and the putative partially functional *pin1-4* protein is in grey. Red arrows indicate measured auxin transport in the basal internode, while red bar-headed lines indicated reduced transport. Black lines represent polarized PIN patterns. Convergence points are marked with asterisks. **(A)** When expressed in both the epidermis and internal tissues with *proAtPIN1* in wildtype Col-0*,* SoPIN1 forms convergent polarization patterns in the epidermis and is partially able to rescue the organ initiation phenotypes and bulk transport in null *pin1-613* mutants. **(B)** When SoPIN1 is expressed only in the epidermis from the *proAtML1* promoter, it forms convergence points in the wildtype background and is able to rescue more fully the organ initiation phenotypes of the *pin1-4* single amino acid change mutation in L*er.* **(C)** In contrast, when PIN1b is expressed in both the epidermis and internal tissues from the *proAtPIN1* promoter in wildtype Col-0, it accumulates mostly in the internal tissues, and is unable to complement the *pin1-613* organ initiation phenotype. It is also unable to transport auxin through stem segments, despite apparently AtPIN1-like accumulation and polarization in the stem. **(D)** When PIN1b is expressed in the epidermis from the *proAtML1* promoter it does not form convergent polarization patterns and is often un-polarized in the wildtype *Ler* background (blue ovals), but it does in the *pin1-4* background, where it is able to rescue the defective organ initiation phenotype and mediate bulk transport. See Figure 7 - supplement 1 for a protein alignment comparing PIN1 protein sequences from diverse angiosperms.

Figure 7 - supplement 1. Brassicaceae-specific PIN1 domains. (A) A wrapped protein alignment showing PIN1 clade members from across the angiosperms. Grass PIN1a proteins are indicated in grey, grass PIN1b proteins are indicated in black and Brassicaceae PIN1 proteins are indicated in red. Domains that are unique to the Brassicaceae family are indicated by transparent red boxes over the alignment. **(B)** Sequenced angiosperm species and version numbers, from https://phytozome.jgi.doe.gov. Species used in the alignment in **(A)** are indicated with green circles. See Figure 7 - Source Data 1 for source data.

Figure 7 - Source Data 1. FASTA alignment source data for Figure 7 - supplement 1.

Table 1. Oligos. See methods for usage.